Electronic Supplementary Information for

A triple helicene based molecular semiconductor characteristic of fully-fused conjugated backbone for perovskite solar cells

Lingyi Fang,‡ Yuyan Zhang,‡ Ming Ren, Xinrui Xie, Tianyu Li, Yi Yuan,* Jing Zhang, and Peng Wang*

State Key Laboratory of Silicon Materials, Department of Chemistry, Zhejiang University, Hangzhou, 310028, China

---

* Corresponding authors.

E-mail addresses: yyuan@zju.edu.cn, pw2015@zju.edu.cn.

‡ These two authors contributed this work equally.

1. Experimental Section

1.1. Materials

2-Aminonaphthalene (99%, Energy Chemical), *N*-chlorosuccinimide (NCS, 98.5%, Energy Chemical), 1,3,5-tribromobenzene (99%, Energy Chemical), palladium diacetate ($Pd(OAc)_2$, 99%, Energy Chemical), bis(2-diphenylphosphinophenyl)ether (DPEPhos, 98%, Energy Chemical), sodium *tert*-butoxide ((*t*-Bu)ONa, 98%, Energy Chemical), tri-*tert*-butylphosphine tetrafluoroborate ($(t\text{-Bu})_3P{\cdot}HBF_4$, 98%, Energy Chemical), potassium carbonate (K_2CO_3, 99%, Energy Chemical), 1-iodohexane (98%, Energy Chemical), iodomethane (99.5%, Energy Chemical), *N*-bromosuccinimide (NBS, 98%, Energy Chemical), 2-chloro-4-methyoxyaniline (99%, Energy Chemical), sodium hydride (NaH, 60% dispersion in mineral oil, Energy Chemical), titanium diisopropoxide bis(acetylacetonate) (TIACA, 75% in isopropanol, Sigma-Aldrich), acetylacetone (ACAC, 99.0%, TCI), TiO_2 paste (30NR-D, Greatcell Solar), caesium iodide (CsI, 99.0%, TCI), methylammonium bromide (MABr, 99.0%, Greatcell Solar), formamidinium iodide (FAI, 99.0%, Greatcell Solar), lead bromide ($PbBr_2$, 99.99%, TCI), lead iodide (PbI_2, 99.99%, TCI), zinc iodide (ZnI_2, 99.995%, Alfa Aesar), hexakis(methoxymethyl)melamine (≥ 98%, Macklin), 1-ethyl-3-methylimidazolium bis(trifluoromethanesulfonyl)imide (EMITFSI, 98%, Energy Chemical), bis(pentamethylcyclopentadienyl)iron (DMFc, 98%, ACROS), ferrocene (Fc, 97%, Aldrich), 4-*tert*-butylpyridine (TBP, 96%, Sigma-Aldrich), and solvents were purchased from commercial resources and used without further purification. 1-Chloronaphthalen-2-amine[1] and 4-*tert*-butylpyridinium bis(trifluoromethanesulfonyl)imide (BPTFSI)[2] were prepared according to the literature methods.

1.2. General Instrumentation

The ^1H and ^{13}C nuclear magnetic resonance (NMR) spectra were measured with an AVANCE III 400 NMR spectrometer (Bruker) or an AVANCE III 500 NMR spectrometer (Bruker). The high resolution mass spectra (HR-MS) were recorded on a 6545 LC/Q-TOF system (Agilent). Attenuated total reflection-Fourier transform infrared (ATR-FTIR) spectra were collected on a Vector 22 FTIR spectrometer (Bruker). The melting points were tested with a WRS-1B automatic digital melting point apparatus (Shanghai INESA Physico-Optical instrument). The single-crystal XRD measurement was performed on a D8 Venture diffractometer (Bruker). The single-crystal structure was defined using the SHELXTL software. The detailed refinement parameters are given in the attached single crystal .cif file. The crystallographic data of TBPC-611 have been deposited to the Cambridge Crystallographic Data Center as supplementary publication no. CCDC-2055713. The cyclic voltammetric measurements were performed with a CHI660C electrochemical workstation (CH Instruments), in conjunction with a three-electrode electrolytic cell equipped with a glassy carbon working electrode, a platinum foil counter electrode, and an Ag/AgCl (sat. KCl) reference electrode. The ultraviolet-visible (UV-Vis) absorption spectra were recorded on a Cary 8454 spectrophotometer (Agilent). The time-resolved photoluminescence (TRPL) traces were recorded with a Life-Spec-II fluorescence spectrometer (Edinburgh). The ultraviolet photoelectron spectra (UPS) were measured with an ESCALAB 250Xi instrument (ThermoFisher). Thickness measurements of thin films were carried out with a D-500 stylus profilometer (KLA-Tencor). Impedance spectra (IS) were measured with an AutolabPGSTAT302N electrochemical workstation by applying a 30 mV voltage perturbation over a series of forward bias potentials to the testing cells in the dark, with the frequency range from 3 MHz to 10 Hz. The electron spin resonance (ESR) spectra were measured on an A300-10/12 spectrometer (Bruker). The differential scanning calorimetric (DSC) analyses were carried out

with a SDT Q600 analyzer (TA Instruments). The scanning electron microscopy (SEM) images were recorded on a SU8010 scanning electron microscope (Hitachi). The X-ray diffraction (XRD) patterns of thin films were measured on a SmartLab diffractometer (Rigaku), using Cu Kα radiation (λ = 0.15405 nm) operated at a power of 7200 W (40 kV, 180 mA). The fluorescence microscopy (FM) images were recorded on an ECLIPSE Ti-U system (Nikon). The external quantum efficiency (EQE) curves were recorded by a Keithley 2400 source meter and an Omni-λ300 monochromator (Zolix, China) equipped with a 150 W xenon lamp (Zolix, China), with a wavelength sampling interval of 10 nm and a current sampling time of 1 s under the full computer control. A Hamamatsu S1337-1010BQ silicon diode for EQE measurements was calibrated at the National Institute of Metrology, China. A Sirius-SS150A solar simulator (Zolix, China) was employed to give an irradiance of 100 mW cm^{-2}. The light intensity was tested with a calibrated monocrystalline silicon solar cell (Model HG-SS20, No. L0013, Beijing Henggong Instrument Co. Ltd., China). Current−voltage (*J*–*V*) characteristics were obtained by applying a bias potential to a testing cell and measuring photocurrent with a Keithley 2400 source meter under the full computer control. The measurements were fully automated using Labview 14.0. A black metal mask with an aperture area of 0.16 cm^2 was covered on a testing cell during all measurements in a dry air-filled glove box.

1.3. Synthesis of TBPC-611

The synthetic route to TBPC-611 is illustrated in Scheme S1 and the preparation details are described as follows.

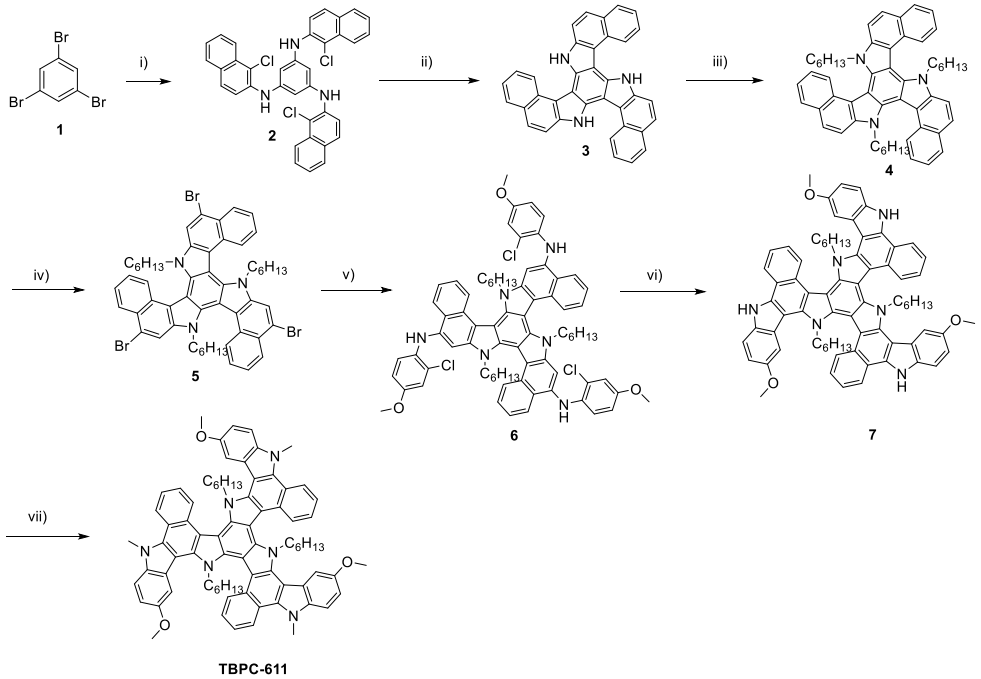

Scheme S1. The synthetic route to TBPC-611. Reagents/conditions: (i) 1-chloronaphthalen-2-amine, $Pd(OAc)_2$, DPEPhos, (*t*-Bu)ONa, toluene, 110 °C, 6 h, 87%; (ii) $Pd(OAc)_2$, $(t\text{-Bu})_3P{\cdot}BF_4$, K_2CO_3, DMAc, 130 °C, 24 h, 85%; (iii) 1-iodohexane, NaH, DMF/THF (*v* : *v* 1:1), rt, 3 h, 98%; (iv) NBS, CH_2Cl_2, 0 °C, 3 h, 99%; (v) 2-chloro-4-methoxyaniline, $Pd(OAc)_2$, DPEPhos, (*t*-Bu)ONa, toluene, 110 °C, 5 h, 86%; (vi) $Pd(OAc)_2$, $(t\text{-Bu})_3P{\cdot}BF_4$, K_2CO_3, DMAc, 130 °C, 48 h, 83%, (vii) iodomethane, NaH, DMF, rt, 0.5 h, 99%.

***N*^{1},*N*^{3},*N*^{5}-Tris(1-chloronaphthalen-2-yl)benzene-1,3,5-triamine (2)**

To a round bottom flask were charged with 1,3,5-tribromobenzene (10.0 g, 30 mmol), 1-chloronaphthalen-2-amine (28.2 g, 150 mmol), $Pd(OAc)_2$ (202 mg, 0.9 mmol), DPEPhos (1.5 g, 2.7 mmol), (*t*-Bu)ONa (14.4 g, 150 mmol), and toluene (250 mL). The mixture was refluxed for 6 h at 110 °C under argon. After cooling to room temperature, the reaction mixture was flashed through a plug of silica gel to remove inorganic salts. The filtrate was collected and concentrated under reduced pressure. The obtained residue was purified by column chromatography (toluene) on alumina to yield a white solid as the desired product **2** (16.7 g, 87% yield). ^{1}H NMR (500 MHz, THF-d_8, δ): 8.09 (d, J = 8.5 Hz, 1H), 7.72 (dt, J = 12.5, 8.5 Hz, 3H), 7.55–7.44 (m, 1H), 7.32 (dd, J = 12.5, 5.5 Hz, 2H), 6.64 ppm (s, 1H). ^{13}C NMR (125 MHz, THF-d_8, δ): 145.86, 139.34, 133.08, 131.00, 129.06, 128.24, 124.74, 123.75, 120.70, 117.41, 104.29 ppm. Anal. calcd for $C_{36}H_{24}Cl_3N_3$: C 71.48, H 4.00, N 6.95; found: C 71.46, H 4.01, N 6.93. HRMS (ESI) *m/z* $[M + K]^+$ calcd for $C_{36}H_{24}Cl_3N_3$, 642.0667; found, 642.0670. Melting point: 260–262 °C. FT-IR (film) ν_{max} = 3047, 3053, 2923, 1595, 1524, 1498, 1472, 1419, 1349, 1294, 1214, 1181, 1057, 988, 944, 805, 746, and 673 cm^{-1}.

14,21-Dihydro-7*H*-benzo[*g*]benzo[4,5]indolo[3,2-*a*]benzo[4,5]indolo[3,2-*c*]carbazole (3)

To a round bottom flask were charged with **2** (12.5 g, 20 mmol), $Pd(OAc)_2$ (674 mg, 3mmol), (*t*-Bu)$_3$P·HBF$_4$ (1.74 g, 6 mmol), K_2CO_3 (25.7 g, 180 mmol), and DMAc (200 mL). The reaction was stirred for 24 h at 130 °C under argon. After cooling to room temperature, the mixture was transferred to a separatory funnel and 50 mL of deionized water was added. The mixture was extracted with three portions of dichloromethane (50 mL each time). The organic layers were combined and the solvent was removed in vacuo. The crude product was then purified by column chromatography (THF/petroleum ether 60–90 °C, *v*/*v*, 1/1) on silica gel to yield a light yellow solid as the desired product **2** (8.7 g, 85% yield). ^{1}H NMR (400 MHz, THF, δ) 11.11 (s, 3H), 9.30 (d, J = 6.6 Hz, 3H), 8.07 (d, J = 6.4 Hz, 3H), 8.01 (d, J = 6.9 Hz, 3H), 7.87 (d, J = 6.9 Hz, 3H), 7.79 (t, J = 6.0 Hz, 3H), 7.51 ppm (t, J = 5.9 Hz, 3H). ^{13}C NMR (100 MHz, THF-d_8, δ): 137.49, 134.82, 131.24, 130.13, 129.83, 126.39, 125.57, 123.53, 118.19, 114.76, 114.72, 106.58 ppm. Anal. calcd for $C_{36}H_{21}N_3$: C 87.25, H 4.27, N 8.48; found: C 87.21, H 4.30, N 8.49. HRMS (ESI) *m/z* $[M]^+$ calcd for $C_{36}H_{21}N_3$, 495.1730; found, 495.1729. Melting point: > 300 °C. FT-IR (film) ν_{max} = 3436, 3046, 2923, 2855, 1672, 1612, 1526, 1461, 1386, 1325, 1248, 1154, 1060, 1001, 862, 801, 745, 687, and 631 cm^{-1}.

7,14,21-Trihexyl-14,21-dihydro-7*H*-benzo[*g*]benzo[4,5]indolo[3,2-*a*]benzo[4,5]indolo[3,2-*c*]carbazole (4)

To a solution of **3** (5.0 g, 10 mmol) in the mixture of DMF and THF (*v*/*v* 1:1) were added 1-iodohexane (5.9 mL, 40 mmol) and NaH (1.6 g, 40 mmol). After stirring at room temperature for 3 h, the mixture was carefully quenched by adding methanol (4 mL). The mixture was poured into water (100 mL) and extracted with three portions of dichloromethane (80 mL each time). The organic layers were combined and the solvent was removed in vacuo. The crude product was then purified by column chromatography (THF/petroleum ether 60–90 °C, *v*/*v*, 1/3) on silica gel to yield a light yellow solid as the desired product **4** (7.4 g, 98% yield). ^{1}H NMR (500 MHz, THF-d_8, δ): 9.13–8.63 (m, 3H), 8.09–7.88 (m, 9H), 7.62–7.55 (m, 3H), 7.50–7.41 (m, 3H), 5.04 (dt, J = 15.1, 7.8 Hz, 3H), 4.71 (ddd, J = 14.6, 7.6, 4.6 Hz, 3H), 1.38–0.01 ppm (m, 33H). ^{13}C NMR (125 MHz, THF-d_8, δ): 141.45, 139.01, 131.40, 130.53, 129.52, 126.96, 126.25, 125.69, 124.16, 119.79, 114.89, 108.59, 50.76, 32.20, 29.21, 27.07, 23.04, 14.32 ppm. Anal. calcd for $C_{54}H_{57}N_3$: C 86.70, H 7.68, N 5.62, found: C 86.73, H 7.69, N 5.65. HRMS (ESI) *m/z* $[M]^+$ calcd for $C_{54}H_{57}N_3$, 747.4553; found, 747.4547. Melting point: 173–176 °C. FT-IR (film) ν_{max} = 2925, 2855, 2341, 1578, 1520, 1462, 1378, 1329, 1189, 1142, 1017, 805, 747, and 689 cm^{-1}.

2,9,16-Tribromo-7,14,21-trihexyl-14,21-dihydro-7*H*-benzo[*g*]benzo[4,5]indolo[3,2-*a*]benzo[4,5]indolo[3,2-

***c*]carbazole (5)**

To a solution of **4** (4.4 g, 6 mmol) in dichloromethane (DCM) was added NBS (3.2 g, 18 mmol) at 0 °C. The mixture was stirred at 0 °C for 3 h, then the mixture was allowed to warm to room temperature and stirred for 30 min. The mixture was then quenched with sodium sulfite aqueous solution (0.1 M, 30 mL). The mixture was transferred to a separatory funnel and 50 mL of deionized water was added. The mixture was extracted with three portions of dichloromethane (50 mL each time). The organic layers were combined and washed with distilled water (100 mL). The solvent was removed in vacuo to afford a yellow solid as the desired product **5** (5.7 g, 99% yield). ^{1}H NMR (400 MHz, THF-d_8, δ): 8.95–8.76 (m, 3H), 8.44 (d, J = 7.3 Hz, 6H), 7.73–7.67 (m, 3H), 7.65–7.59 (m, 3H), 4.90 (dt, J = 15.1, 7.7 Hz, 3H), 4.73 (ddd, J = 14.6, 7.6, 4.6 Hz, 3H), 1.37–0.23 ppm (m, 33H). ^{13}C NMR (100 MHz, THF-d_8, δ): 141.16, 139.14, 130.93, 128.98, 128.61, 127.24, 126.78, 125.79, 120.01, 119.66, 119.30, 108.26, 50.91, 32.19, 29.39, 27.09, 23.08, 14.34 ppm. Anal. calcd for $C_{54}H_{54}Br_3N_3$: C 65.86, H 5.53, N 4.27; found: C 65.87, H 5.54, N 4.25. HRMS (ESI) *m/z* $[M]^+$ calcd for $C_{54}H_{54}Br_3N_3$, 983.1847; found, 983.1844. Melting point: 273–275 °C. FT-IR (film) ν_{max} = 3503, 2954, 2927, 2856, 1568, 1515, 1460, 1331, 1274, 1157, 1093, 1067, 907, 851, 757, 689, 659, and 618 cm^{-1}.

***N*^{2},*N*^{9},*N*^{16}-Tris(2-chloro-4-methoxyphenyl)-7,14,21-trihexyl-14,21-dihydro-7*H*-benzo[*g*]benzo[4,5]indolo[3,2-*a*]benzo[4,5]indolo[3,2-*c*]carbazole-2,9,16-triamine (6)**

A mixture of **5** (5.0 g, 5 mmol), 2-chloro-4-methyoxyaniline (4.0 g, 25 mmol), $Pd(OAc)_2$ (33.7 mg, 0.15 mmol), DPEPhos (242.3 mg, 0.45 mmol), (*t*-Bu)ONa (2.4 g, 25 mmol), and toluene (100 mL) in a round bottom flask was stirred for 5 h at 110 ºC under argon. After cooling to room temperature, the mixture was transferred to a separatory funnel and 100 mL of deionized water was added. The mixture was extracted with three portions of dichloromethane (100 mL each time). The organic layers were combined and the solvent was removed in vacuo. The crude product was then purified by column chromatography (THF/petroleum ether 60–90 °C, *v*/*v*, 1/1) on silica gel to yield a light yellow solid as the desired product **6** (5.3 g, 86% yield). ^{1}H NMR (500 MHz, THF-d_8, δ): 8.92 (t, J = 47.7 Hz, 3H), 8.26 (d, J = 8.3 Hz, 3H), 7.66 (s, 3H), 7.57 (t, J = 7.3 Hz, 3H), 7.42 (t, J = 7.5 Hz, 3H), 7.11 (d, J = 2.7 Hz, 3H), 7.06–6.99 (m, 6H), 6.77 (dd, J = 8.9, 2.8 Hz, 3H), 4.94 (dt, J = 15.0, 7.7 Hz, 3H), 4.56–4.47 (m, 3H), 3.78 (s, 9H), 1.32–1.19 (m, 6H), 0.85–0.31 ppm (m, 27H). ^{13}C NMR (125 MHz, THF-d_8, δ): 155.49, 142.15, 138.75, 138.13, 137.42, 131.23, 127.38, 126.07, 125.95, 124.78, 124.16, 123.78, 121.12, 116.27, 116.04, 114.83, 109.01, 106.50, 56.16, 50.71, 32.28, 29.08, 27.05, 23.09, 14.42 ppm. Anal. calcd for $C_{75}H_{75}Cl_3N_6O_3$: C 74.15, H 6.22, N 6.92; found: C 74.13, H 6.23, N 6.90. HRMS (ESI) *m/z* $[M]^+$ calcd for $C_{75}H_{75}Cl_3N_6O_3$, 1212.4966; found, 1212.4963. Melting point: 131–133 °C. FT-IR (film) ν_{max} = 3382, 2932, 1579, 1501, 1461, 1345, 1278, 1211, 1103, 1043, 861, 806, and 758 cm^{-1}.

5,15,25-Trihexyl-3,13,23-trimethoxy-10,20,30-3*H*-5,10,15,20,25,30-hexahydrobenzo[*c*]benzo[4,5]indene[2',1':6,7]indolo[2,3-*g*]benzo[4,5]indolo[2',1':6,7]indolo[2,3-i]indeno[1,2-*a*]carbazole (7)

To a round bottom flask were charged with **6** (5.0 g, 4.1 mmol), $Pd(OAc)_2$ (148 mg, 0.66 mmol), (*t*-Bu)$_3$P·HBF$_4$ (356.2 mg, 1.23 mmol), K_2CO_3 (5.1 g, 36 mmol), and DMAc (50 mL). The reaction was stirred for 48 h at 130 °C under argon. After cooling to room temperature, the mixture was transferred to a separatory funnel and 50 mL of deionized water was added. The mixture was extracted with three portions of dichloromethane (50 mL each time). The organic layers were combined and the solvent was removed in vacuo. The crude product was then purified by column chromatography (THF/petroleum ether 60–90 °C, *v*/*v*, 1/1) on silica gel to yield a light

yellow solid as the desired product **7** (3.8 g, 83% yield). ^{1}H NMR (500 MHz, THF-d_8, δ): 11.44 (d, J = 14.6 Hz, 3H), 10.19 (dd, J = 18.9, 8.4 Hz, 2H), 9.96 (d, J = 8.3 Hz, 0H), 9.78 (d, J = 8.2 Hz, 1H), 8.57 (t, J = 7.0 Hz, 3H), 8.34–8.14 (m, 3H), 7.90 (ddd, J = 13.1, 11.5, 6.7 Hz, 3H), 7.67 (ddd, J = 16.7, 9.5, 5.8 Hz, 6H), 7.26–7.04 (m, 3H), 5.49–5.28 (m, 1H), 5.21–4.76 (m, 5H), 4.22 (d, J = 1.2 Hz, 5H), 4.15 (d, J = 6.4 Hz, 4H), 0.86–0.07 ppm (m, 33H). ^{13}C NMR (125 MHz, THF-d_8, δ): 155.70, 155.65, 155.61, 142.42, 141.87, 141.44, 141.25, 140.31, 140.30, 140.17, 139.75, 139.74, 139.39, 139.38, 138.66, 137.99, 137.83, 135.89, 135.68, 135.52, 130.11, 130.00, 129.87, 128.41, 127.45, 127.44, 125.54, 125.31, 125.13, 124.27, 124.21, 123.90, 123.64, 123.61, 123.49, 123.13, 123.02, 122.93, 120.99, 120.83, 120.79, 117.45, 116.36, 115.15, 115.05, 114.89, 114.58, 114.47, 112.92, 110.78, 109.78, 105.97, 105.83, 105.26, 56.69, 56.44, 54.75, 54.27, 53.83, 32.50, 32.25, 31.95, 31.79, 28.22, 27.58, 27.44, 27.11, 27.02, 26.87, 23.22, 23.06, 22.92, 14.17, 14.02, 14.00 ppm. Anal. calcd for $C_{75}H_{72}N_6O_3$: C 81.49, H 6.57, N 7.60; found: C 81.50, H 6.56, N 7.59. HRMS (ESI) m/z $[M]^+$ calcd. for $C_{75}H_{72}N_6O_3$, 1104.5666; found, 1104.5661. Melting point: 268–270 °C. FT-IR (film) ν_{max} = 3425, 2953, 2925, 2855, 1720, 1622, 1578, 1527, 1461, 1377, 1326, 1292, 1211, 1165, 1114, 1032, 939, 803, 757, 734, 685, and 618 cm^{-1}.

5,15,25-Trihexyl-3,13,23-trimethoxy-10,20,30-trimethyl-5,10,15,20,25,30-hexahydrobenzo[*c*]benzo[4,5]indene[2',1':6,7]indolo[2,3-*g*]benzo[4,5]indolo[2',1':6,7]indolo[2,3-i]indeno[1,2-*a*]carbazole (TBPC-611)

To a round bottom flask were charged with **7** (3.5 g, 3.2 mmol), NaH (2.2 g, 32 mmol), iodomethane (1.0 mL, 16 mmol), and DMF (50 mL). The mixture was stirred for 30 min at room temperature. Then 5 mL of methanol was slowly added to quench the reaction. The resulting mixture was poured into water (50 mL) and extracted with three portions of dichloromethane (50 mL each time). The organic layers were combined and the solvent was removed in vacuo. The crude product was then purified by column chromatography (THF/petroleum ether 60–90 °C, *v*/*v*, 1/3) on silica gel to yield a yellow solid as the desired product **TBPC-611** (3.6 g, 99%). ^{1}H NMR (500 MHz, THF-d_8, δ): 10.36 (d, J = 8.5, 1H), 10.26 (dd, J = 8.4, 1.2 Hz, 1H), 10.06 (d, J = 8.3 Hz, 0H), 9.84 (dd, J = 8.2, 1.3 Hz, 1H), 8.99 (dd, J = 8.3, 2.4 Hz, 3H), 8.47–8.22 (m, 3H), 8.04–7.85 (m, 3H), 7.82–7.52 (m, 6H), 7.37–7.19 (m, 3H), 5.34 (ddd, J = 14.4, 9.6, 4.8 Hz, 1H), 5.08–4.95 (m, J = 27.3, 14.1, 9.1, 5.4 Hz, 2H), 4.90 (ddd, J = 15.0, 9.9, 5.9 Hz, 1H), 4.79 (ddd, J = 14.4, 9.4, 5.3 Hz, 1H), 4.68–4.50 (m, 10H), 4.23 (d, J = 10.8 Hz, 6H), 4.16 (d, J = 3.2 Hz, 3H), 1.36–1.26 (m, 2H), 0.77–0.06 ppm (m, 31H). ^{13}C NMR (125 MHz, THF-d_8, δ): 155.91, 155.83, 155.77, 142.45, 141.87, 141.36, 140.03, 140.03, 139.77, 138.74, 138.38, 137.96, 137.81, 137.75, 137.55, 131.26, 131.15, 130.78, 128.67, 127.31, 127.28, 126.06, 125.42, 125.30, 124.83, 124.75, 124.69, 124.29, 124.08, 123.69, 123.67, 122.56, 122.35, 122.27, 122.24, 121.69, 121.66, 118.16, 117.58, 117.25, 115.94, 115.08, 114.87, 114.66, 114.23, 111.36, 111.35, 111.29, 111.27, 110.28, 110.19, 106.37, 106.18, 105.44, 56.95, 56.67, 56.56, 54.23, 53.95, 53.75, 35.51, 35.26, 35.10, 32.18, 31.92, 31.77, 27.92, 27.59, 27.41, 27.10, 27.01, 26.98, 23.19, 23.05, 22.91, 14.14, 14.00, 13.96 ppm. Anal. calcd for $C_{78}H_{78}N_6O_3$: C 81.64, H 6.85, N 7.32, found: C 81.61, H 6.87, N 7.30. Melting point: > 300 °C. HRMS (ESI) m/z $[M]^+$ calcd for $C_{78}H_{78}N_6O_3$, 1146.6130; found, 1146.6131. FT-IR (film) ν_{max} = 2926, 2857, 1620, 1577, 1530, 1484, 1400, 1327, 1299, 1237, 1211, 1167, 1106, 1035, 844, 795, 758, and 684 cm^{-1}.

1.4. Single Crystal Growth

Single crystals of TBPC-611 were grown from a nearly saturated solution of dichloromethane and heptane at

room temperature, by slowly evaporating the solvent.

1.5. Electrical Conductivity

The current–voltage (*I–V*) curve in the bias range from −1.5 V to 1.5 V of an organic thin film deposited on the interdigitated gold electrodes was measured to derive the direct-current electrical conductivity (σ). The number (n) of channels in the interdigitated electrodes on SiO_2 is 119, the channel length (L) is 1.5 mm, the channel width (W) is 10 μm, and the channel thickness (t) is 110 nm. The organic film was spin-coated from a chlorobenzene solution of TBPC-611 or spiro-OMeTAD (35 mg mL^{-1}) at a spin speed of 2000 rpm. To enhance the doping level, 132 mM of TBP and 15% of BPTFSI were added. The device was stored in dry air (< 5% RH) for 7 d before measurement. *I–V* curve was recorded on a CHI660C electrochemical workstation. The σ was calculated by equation

$$\sigma = s\frac{W}{nLt}, \tag{1}$$

where s is the slope derived from the linear fitting of *I–V* plot.

1.6. Hole Density

The hole density of an organic film was estimated from impedance measurement on the metal–insulator–semiconductor (MIS) device,[3] with a structure of n^{++}-Si/SiO_2/benzocyclobutene/organic film/Au. Benzocyclobutene (BCB) was spin-coated on top of the SiO_2 dielectric layer from a 1 mg mL^{-1} solution at 4000 rpm and then was annealed at 250 °C for 1 h. The organic semiconductor layer was formed by spin-coating an 80 mg mL^{-1} tetrahydrofuran solution at 1200 rpm on top of BCB after cooling, followed by thermal evaporation of the gold contact (120 nm). The n^{++}-Si was used as the working electrode. The stack of SiO_2 and BCB was served as the insulator layer. The MIS device was tested using an AutolabPGSTAT302N electrochemical workstation. The impedance spectra were measured over a wide frequency range (10 Hz – 3 MHz) with a small perturbation of 30 mV and various biases from −10 to 10 V. Capacitance–frequency spectra of the MIS device at different bias can be calculated from the real and imaginary parts of the measured impedance, corrected by the effect of series resistance (R_s) and parasitic inductance (L_i) that is dominant at high frequencies. The corrected capacitance (C_{cor}) can be derived from equation

$$C_{cor} = -\frac{1}{\omega}\left[\frac{Z'' - \omega L_i}{(Z' - R_s)^2 + (Z'' - \omega L_i)^2}\right], \tag{2}$$

where Z' and Z'' are the real and imaginary parts of the measured impedance, respectively, and ω is the angular frequency. In the accumulation regime (large negative bias) and at low frequencies, the total C_{cor} of the

MIS device should be equal to the insulator capacitance (C_i). The larger C_{cor}, measured at low frequencies, originates from parasitic processes (a lateral spread of charge carriers, traps, leakage current), which can follow the low-frequency signal and thus, contributes to the measured C_{cor}. At higher frequencies the effect is negligible. However, the capacitance effect of the neutral region of the active layer, connected in series, reduces the C_{cor} of the MIS device with increasing frequency. The C_{cor} can be obtained by equation,

$$C_{cor} = \frac{1}{\frac{1}{C_i} + \frac{1}{C_s}} = \frac{C_i C_s}{C_i + C_s}, \tag{3}$$

where C_s is the capacitance of the semiconductor layer. The capacitance–voltage (C–V) characteristics obtained at the medium frequency clearly reveals two distinct regimes of accumulation and depletion. The free hole density (p) can be derived from the slope of the Mott-Schottky plot,

$$p = \frac{2}{q\varepsilon_r\varepsilon_0 \frac{d(A/C)^2}{dV}}, \tag{4}$$

where q is the elementary charge, ε_r is the relative permittivity, ε_0 is the vacuum permittivity, and A is the area of the MIS device. Hole mobility, μ_h, can be further calculated by equation,

$$\mu_h = \frac{\sigma}{p \times q}. \tag{5}$$

1.7. Hole Mobility of Hole-Only Device

A laser etched indium-doped tin-oxide (ITO) glass was used as the substrate of the hole-only device. The substrate was cleaned in ultrasonic baths in the order of Hellmanex (2%, deionized water), deionized water, acetone, and ethanol. A 40-nm-thick PEDOT:PSS layer was then spin-coated onto the substrate and annealed at 150 °C for 15 min in air. A flat thin film of TBPC-611 or spiro-OMeTAD was further spun from an 80 mg mL^{-1} tetrahydrofuran solution at 5000 rpm for 30 s. To enhance the doping level, 132 mM of TBP and 15% of BPTFSI were added. Finally, a 120-nm-thick gold layer was evaporated under < 10^{-4} Pa vacuum. The current density–voltage (J–V) curve of the hole-only device was measured in the dark with a Keithley 2400 source-measure unit in a dry air-filled glovebox. The μ_h was derived by fitting J–V curve with equation,[4,5]

$$J = \frac{9}{8}\varepsilon_0\varepsilon_r\mu_h\frac{V^2}{d^3}, \tag{6}$$

where d is the thickness of a hole-transport layer.

1.8. Fabrication, Encapsulation, and Dismantling of Solar Cells

A laser etched fluorine doped tin oxide (FTO) glass (TEC 14, Nippon Sheet Glass Co., Ltd, white glass, 1.6 mm

thickness) was rinsed in turn with detergent, deionized water, acetone, and ethanol for 10 min, using an ultrasonic bath. Whereafter, a compact TiO_2 blocking layer was deposited onto the FTO glass at 450 °C via spray pyrolysis of an alcoholic solution of TIACA (40 mM) and ACAC (400 mM). Next, a mesoporous TiO_2 layer at the thickness of ~200 nm was coated by spin-coating of a TiO_2 colloidal solution at 4000 rpm for 10 s, with a ramp rate of 2000 rpm s^{-1}. The TiO_2 solution was prepared in advance by diluting the commercial TiO_2 paste (30NR-D) with anhydrous ethanol at a weight ratio of 1:6. After solidification at 100 °C in air for 10 min, the mesoporous film was afforded via sintering at 450 °C with a flow of dry air for 30 min to wipe off all carbon components. The deposition of a CsMAFA perovskite film was carried out with two-step spin-coating at 2000 rpm for 10 s (ramp rate 200 rpm s^{-1}) and 6000 rpm for 30 s (ramp rate 2000 rpm s^{-1}), in a dry air-filled glove box with < 5% humidity. Note that 150 μL CB was dripped on the substrate at the time of 15 s before the spin end. The deposited film was subsequently annealed at 120 °C for 1 h to generate the black perovskite. The perovskite precursor solution was prepared by dissolving 1.3 M PbI_2, 1.2 M FAI, 0.1 M $PbBr_2$, 0.1 M MABr, and 0.07 M CsI in the mixed solvent of DMSO and DMF (*v*:*v*, 1:4). Next, 50 μL IPA solution of ZnI_2 (4 mg mL^{-1}) was dropped on the top of the perovskite film at 2500 rpm for 25s. The film was then annealed at 80 °C in the dark for 10 min. Subsequently, the IPA solution of hexakis(methoxymethyl)melamine (2 mg mL^{-1}) was spin-coated onto the perovskite layer, producing an ultrathin layer of melamine-formaldehyde resin after heating at 80 °C for 10 min. The HTL was then deposited by dynamic spin-coating at 4000 rpm for 30 s with a ramp rate 2000 rpm s^{-1}. The solution is composed of 35 mg mL^{-1} TBPC-611 (or spiro-OMeTAD), and 132 mM TBP in chlorobenzene, and the thickness of TBPC-611 (or spiro-OMeTAD) is ~50 nm. To enhance the doping level, 15% of BPTFSI was added. Under the vacuum of ≤ 1×10^{-4} Pa, the gold electrode was thermally deposited by use of a shadow mask. The thickness of gold layer was ~120 nm. The device was stored in dry air (< 5% RH) overnight, laminated with a waterproof adhesive tape, and further encapsulated by an epoxy adhesive (3M). The hermetically sealed cell is referred as "fresh cell" in the main text. The cell active area is ~0.5 × 0.5 cm^2. For fundamental characterizations, the sealing materials, gold electrode, and HTL were removed if necessary

1.9. Preparation of Perovskite Samples on Alumina for PL Measurements

A 1.2-mm thick glass slide (25 mm × 16 mm) was rinsed in turn with detergent, deionized water, acetone, and ethanol for 10 min using an ultrasonic bath. A mesoporous alumina film was deposited by spin-coating of a diluted colloidal dispersion (5 wt %) of Al_2O_3 nanoparticles in isopropanol (IPA) for 60 s at 5000 rpm, onto a cleaned glass substrate. The films were dried at 150 °C for 10 min. The perovskite layer was

deposited onto the alumina substrate with the same protocol for PSC fabrication. A solution of 15 mg mL^{-1} PVK in chlorobenzene or 35 mg mL^{-1} molecular semiconductor was then spin-coated atop the annealed perovskite film at 5000 rpm for 30 s. Next, a gold layer at the thickness of ~120 nm was thermally evaporated under a vacuum of ≤ 10^{-4} Pa. The samples were also sealed according to the same method for PSCs.

1.10. Stability Tests

The sealed PSCs and control samples were kept in the air-filled FD56 oven (Binder, Germany) set at 85 °C. The environmental RH of our lab was in the range of 45–90%. The cells were taken out at regular interval for *J–V* measurements. The operation stability of PSCs was measured via maximum power point (MPP) tracking of PSCs at 55 °C under continuous illumination of an one sun equivalent LED array with a PVLT-G8001M-256H test system in a nitrogen-filled glovebox. The MPP data were updated every 15 min using a standard perturb and observe method.

2. Theoretical Modeling

2.1. Molecular Geometry and Energy Level

We performed the density functional theory (DFT) calculations by use of the Gaussian 09 program suite, with the 6-311G(d,p) basis set for all atoms. We employed the integral equation formalism polarizable continuum model (IEFPCM) to model the solvent (THF) effect.[6] We optimized the ground-state geometry by use of the popular B3LYP exchange-correlation functional.[7]

2.2. Modeling Glass Transition Temperature

By use of the amorphous cell module in the Materials Studio package,[8] boxes with periodic boundary for the solid of 400 organic semiconductor molecules and the composite of 400 organic semiconductor molecules and 200 BPTFSI molecules were constructed. The force field of condensed-phase optimized molecular potential for atomistic simulation studies II (COMPASS II)[9] was utilized for molecular semiconductor (MD) simulations. In the COMPASS II force field, the potential energy (E_{pot}) is described by

$$E_{pot} = E_{bond} + E_{cross} + E_{non}, \quad (7)$$

where E_{bond}, E_{cross}, and E_{non} are the bonded energy, the cross energy, and the nonbonded energy, respectively. We started MD simulations from 700 K under the canonical ensemble for 1 ns total simulation time with 1 fs time step by a Nose thermostat. Next, the simulation was carried out for another 1 ns under isothermal-isobaric ensemble by keeping the pressure at 1 atm. The temperature was decreased to 250 K at the 20 K interval during

the simulations with the FORCITE module in the Materials Studio package. We derived the T_g^{MD} value from the crossing point of linear fittings of specific volume at the high and low temperature regions.

2.3. Simulation of Solubility Coefficient, Diffusion Coefficient, and Permeability Coefficient

2.3.1. Solubility Coefficient

Generally, the adsorption isotherm of small gas molecules in the organic composite is nonlinear, which can be described by the following formula,

$$C = C_D + C_H, \tag{8}$$

where C is the total adsorption amount of gas molecules in the organic composite, C_D is the adsorption amount of gas molecules in the densely packed region, and C_H is the adsorption amount of gas molecules in the region of filling defects or micropores. C_D and C_H are respectively defined by equations 9 and 10,

$$C_D = k_D p, \tag{9}$$

$$C_H = C'_H \frac{bp}{1+bp}, \tag{10}$$

where p is the pressure, k_D is the Henry's law constant, C'_H is the Langmuir volume constant, and b is the Langmuir affinity constant. In the pressure range of 10−100 kpa, we performed a series of GCMC simulations on amorphous boxes at a given pressure, and obtained the adsorption isotherm of adsorption amount as a function of pressure. The solubility coefficient (S) can be expressed as

$$S = \frac{C}{p}, \tag{11}$$

where S is derived from the limit slope when the pressure is zero, by the following expression,

$$S = \lim_{p \to 0} \frac{C}{p}. \tag{12}$$

2.3.2. Diffusion Coefficient

In order to model the physical diffusion of CH_3I or H_2O, we inserted 40 extra gas molecules into the above constructed boxes. Heating and cooling cycle processes were followed in the isothermal-isobaric ensemble, within the temperature range from 300 to 700 K at 25 K interval. Next, MD simulations in the isothermal-isobaric ensemble (333 K, 1 bar) were performed for 1 ns. At the end, MD simulation in the canonical ensemble (333 K) was performed for 1 ns to track the diffusion trajectories. The diffusion coefficient (D) can be estimated by

$$D = \frac{1}{6N} \lim_{t \to \infty} \frac{\mathrm{d}}{\mathrm{d}t} \left\langle \sum_i^N [r_i(t) - r_i(0)]^2 \right\rangle, \tag{13}$$

where N is the number of gas molecules while $r_i(t)$ and $r_i(0)$ refer to the final and initial positions of the mass centers of gaseous molecules over the time interval (t), respectively. The term of $\sum_i^N [r_i(t) - r_i(0)]^2$ means the ensemble average of mean square displacement.

2.3.3. Permeability Coefficient

The permeability coefficient of gas molecules (P) can be expressed as

$$P = S \times D, \tag{14}$$

where S reflects the thermodynamic characteristics of the interaction between the permeating molecules and the organic composite, and D reflects the dynamic characteristics of the permeating molecules in the system.

3. Reference

1 N. Zhao, L. Qiu, X. Wang, Z. An and X. Wan, *Tetrahedron Lett.*, 2014, **55**, 1040.

2 Y. Ren, M. Ren, X. Xie, J. Wang, Y. Cai, Y. Yuan, J. Zhang and P. Wang, *Nano Energy*, 2021, **81**, 105655.

3 N. F. Mott and R. W Gurney, *Electronic Processes in Ionic Crystals 1st edn*, Oxford University Press, 1940.

4 P. N. J. Murgatroy, *J. Phys. D: Appl. Phys.*, 1970, **3**, 151.

5 B. Yurash, D. X. Cao, V. V. Brus, D. Leifert, M. Wang, A. Dixon, M. Seifrid, A. E. Mansour, D. Lungwitz, T. Liu, P. J. Santiago, K. R. Graham, N. Koch, G. C. Bazan and T.-Q. Nguyen, *Nat. Mater.*, 2019, **18**, 1327.

6 A. Klant, C. Moya and J. Palomar, *J. Chem. Theory Comput*., 2015, **11**, 4220.

7 A. D. Becke, *J. Chem. Phys.*, 1993, **98**, 1372.

8 Materials Studio, Accelrys Software, Inc, San Diego, CA, 2014.

9 H. Sun, Z. Jin, C. Yang, R. L. C. Akkermans, S. H. Robertson, N. A. Spenley, S. Miller and S. M. Todd, *J Mol. Model.*, 2016, **22**, 47.

4. Additional Data

Table S1 Single crystal data of TBPC-611

Compound	TBPC-611
Empirical formula	$C_{78}H_{78}N_6O_3$
Formula weight	1147.47
Wavelength [Å]	1.34138
Crystal system	Triclinic
Space group	$P\bar{1}$
a [Å]	14.2538 (6)
b [Å]	17.1903 (7)
c [Å]	17.3592 (7)
α [°]	79.038 (2)
β [°]	72.546 (2)
γ [°]	68.828 (2)
Volume [Å^3]	3767.7 (3)
Z	2
ρ_{calc} [g cm^{-3}]	1.012
μ [mm^{-1}]	0.305
F [000]	1224.0
Crystal size [mm^3]	0.2×0.18×0.06
2Θ range for data collection [°]	2.408 to 48.455
Refl. Collected	60426
Independent reflections	15322
Data/restraints/parameters	15322/199/868
Data completeness	0.993
Goodness-of-fit on F^2	1.130
Final *R* indexes [I>=2σ (I)]	R1 = 0.0949, wR2 = 0.2951
Final *R* indexes [all data]	R1 = 0.1545, wR2 = 0.3382
Largest diff. peak/hole [e Å^{-3}]	0.667/–0.533
CCDC deposition number	2055713

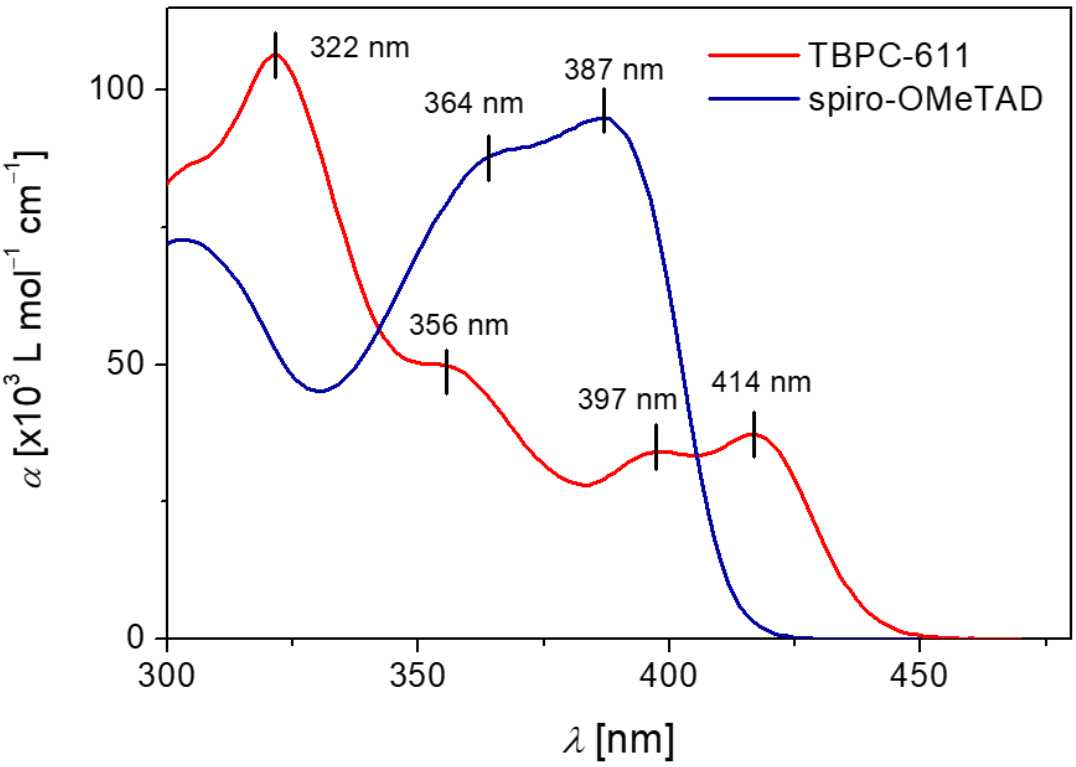

Fig. S1 The UV-vis absorption spectra of TBPC-611 and spiro-OMeTAD in THF (50 μM).

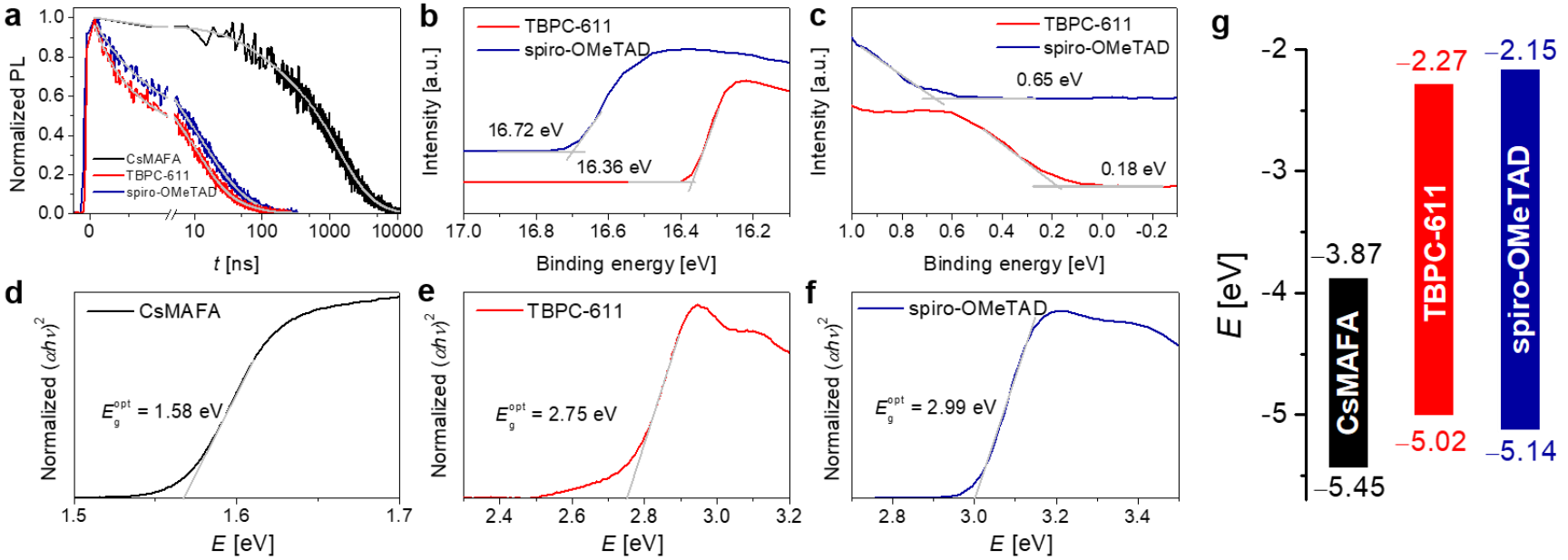

Fig. S2 (a) The TRPL traces. The gray lines are biexponential fittings. b,c) The ultraviolet photoelectron spectra (UPS) of thin films deposited on FTO in the cutoff (b) and onset (c) energy regions. The HOMO energy levels are derived, being –5.02 eV for TBPC-611 and –5.14 eV for spiro-OMeTAD, both of which are over 0.3 eV higher than the valence band edge of –5.45 eV for CsMAFA. (d–f) The Tauc plots of thin films of CsMAFA, TBPC-611, and spiro-OMeTAD. The derived optical gaps (E_g^{opt}) are also included. (g) The energy diagram of CsMAFA, TBPC-611, and spiro-OMeTAD. The driving force of hole extraction (ΔG_0) is derived as 430 meV with TBPC-611 and 310 meV with spiro-OMeTAD. In addition, the energy diagram also suggests the energetic role of electron blocking by either TBPC-611 or spiro-OMeTAD.

Table S2 The fitting parameters of TRPL decays, time constants of hole extraction, and yields of hole extraction[a]

Sample	τ_1 [ns]	A_1	τ_2 [ns]	A_2	$\bar{\tau}$ [ns]	ϕ_h [%]	τ_h [ns]
Al_2O_3/CsMAFA/PVK	224	0.27	1641	0.73	1258	/	/
Al_2O_3/CsMAFA/TBPC-611	24	0.39	5	0.61	12	99.0	12
Al_2O_3/CsMAFA/spiro-OMeTAD	36	0.45	6	0.55	20	98.4	20

[a] τ_1 and τ_2 are the time constants of fast and slow decays, A_1 and A_2 are the relative amplitudes of fast and slow decays, and $\bar{\tau}$ is the amplitude-averaged time constant which is calculated by equation $\bar{\tau} = A_1\tau_1 + A_2\tau_2$. τ_h is the time constant of hole extraction derived with equation $\tau_h = \frac{\bar{\tau}_{PVK} \times \bar{\tau}_{HTL}}{\bar{\tau}_{PVK} - \bar{\tau}_{HTL}}$, and ϕ_h is the yield of hole extraction derived with equaltion $\phi_h = \frac{\bar{\tau}_{PVK} - \tau_h}{\bar{\tau}_{PVK}}$, where $\bar{\tau}_{PVK}$ is the amplitude-averaged time constant of the PVK-covered CsMAFA on the alumina substrate, and $\bar{\tau}_{HTL}$ is the amplitude-averaged time constant of HTL-covered CsMAFA on the alumina substrate.

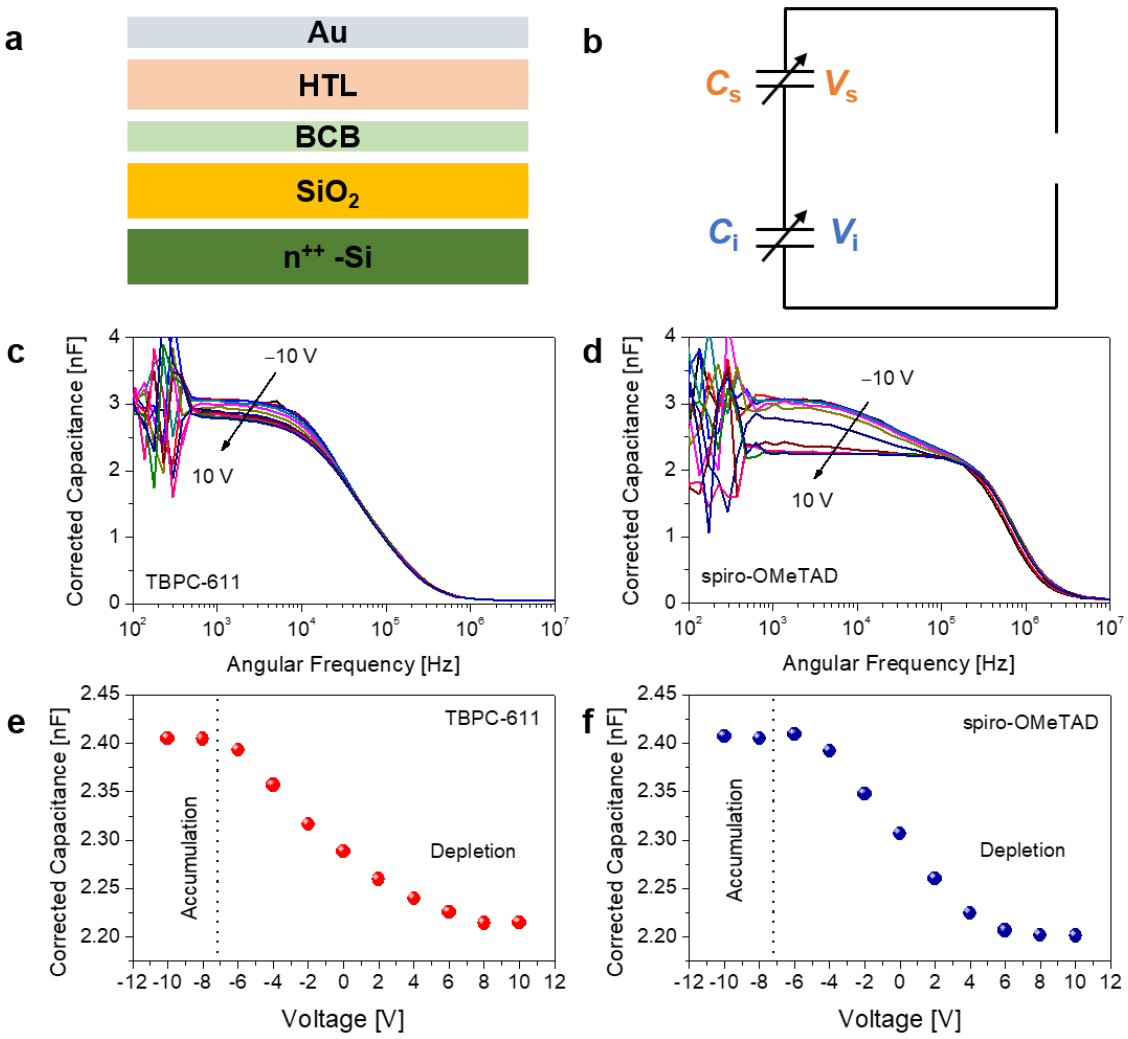

Fig. S3 (a) The schematics of the MIS device. (b) The equivalent circuit of the MIS device. (c,d) Plots of the corrected capacitance derived from impedance measurement of the MIS device with the neat TBPC-611 or spiro-OMeTAD layer as a function of the angular frequency. The bias voltage for impedance measurement is ranged from −10 V to +10 V. (e,f) Plots of the corrected capacitance at 10 kHz as a function of the bias voltage.

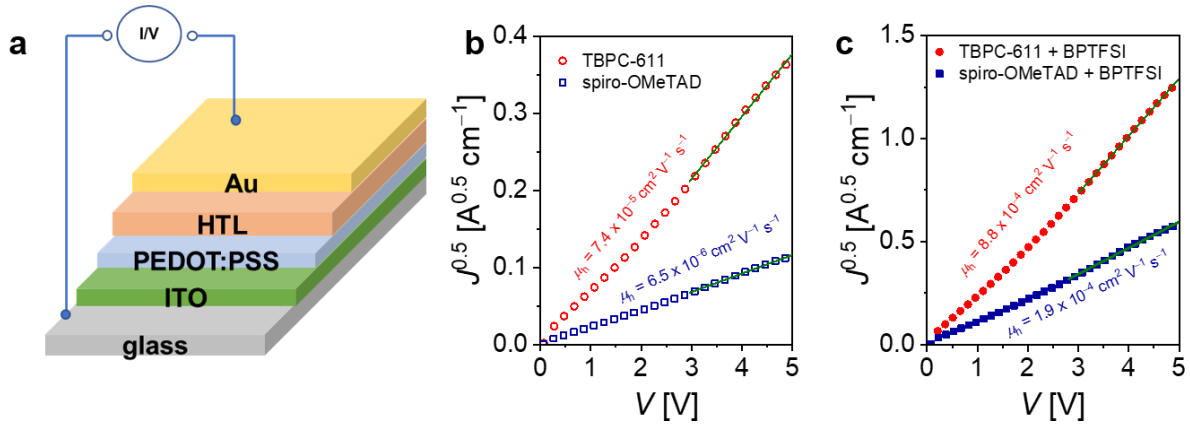

Fig. S4 (a) The schematics of the hole-only device. (b) The typical *J*–*V* curve of the hole-only device with the neat film of TBPC-611 or spiro-OMeTAD. (c) The typical *J*–*V* curve of the hole-only device with the 15% BPTFSI-containing film of TBPC-611 or spiro-OMeTAD. In panel b and c, the gray line in the range of 3–5 V is the fitting by the equation $J = \frac{9}{8}\varepsilon_0\varepsilon_r\mu_h\frac{V^2}{d^3}$, where ε_0 is the vacuum permittivity, ε_r is the relative permittivity, μ_h is the mobility, and d is the film thickness.

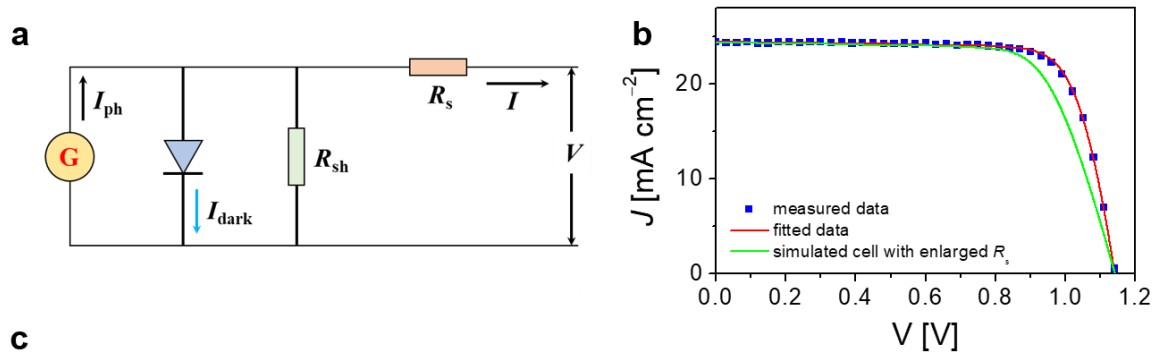

c

PSC	R_{sh} [kΩ]	I_s [A]	R_s [Ω]	n	I_{ph} [mA]	J_{SC} [mA cm^{-2}]	V_{OC} [V]	FF [%]	PCE [%]
spiro-OMeTAD/measured	/	/	/	/	/	24.5	1.140	77.2	21.6
spiro-OMeTAD/simulated	10.1	1.4×10^{-14}	15.6	1.68	3.91	24.5	1.139	77.7	21.6
Simulated cell with enlarged R_s	10.1	1.4×10^{-14}	35	1.68	3.91	24.4	1.139	72.1	20.0

Fig. S5 (a) The Shockley equivalent circuit of a solar cell. G is the photocurrent generator, I_{dark} is the dark current, R_s is the series resistance, R_{sh} is the shunt resistance, and I_{ph} is the photogeneration current. The I–V curve of a solar cell can be fitted by use of equation, $I = \frac{1}{1+R_s/R_{sh}}\left\{I_s\left[\exp\frac{e(V-IR_s)}{nk_BT}-1\right]+\frac{V}{R_{sh}}-I_{ph}\right\}$, where I_s is the reverse saturation current, n is the ideality factor, k_b is the Boltzmann constant, T is the absolute temperature, and e is the elementary charge. (b) The measured (dotted blue) and fitted (red line) J–V data of the typical PSC with the 15% BPTFSI-containing composite of spiro-OMeTAD. According to the conductivities of the neat TBPC-611 film and the BPTFSI-containing composite film of spiro-OMeTAD, R_s is enlarged from 15.6 to 149 Ω, producing the simulated green curve of a bad solar cell. (c) Experimental and fitted photovoltaic parameters. The fitting parameters are also included.

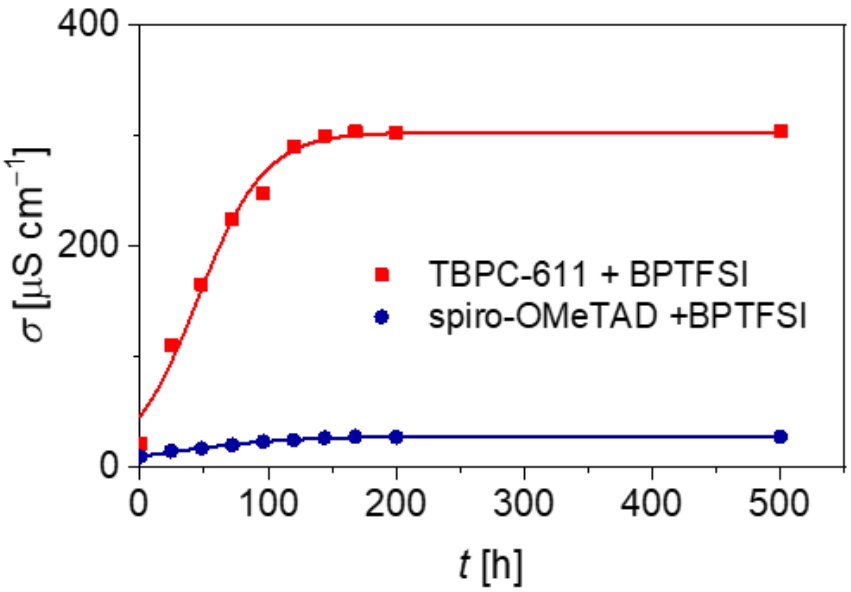

Fig. S6 The electrical conductivity (σ) evolution of BPTFSI containing composite TBPC-611 and spiro-OMeTAD films stored at room temperature in dry air (< 5% RH).

Table S3 The electrical conductivity (σ), hole density (p), and hole mobility (μ_h) of the neat or 15% BPTFSI-containing film of TBPC-611 or spiro-OMeTAD[a]

Sample	σ [μS cm^{-1}]	p [cm^{-3}]	μ_h^{σ} [cm^2 V^{-1} s^{-1}]	μ_h^{SCLC} [cm^2 V^{-1} s^{-1}]
Neat TBPC-611	9.4×10^{-1}	4.0×10^{17}	1.5×10^{-5}	7.4×10^{-5}
Neat spiro-OMeTAD	8.5×10^{-2}	2.9×10^{17}	1.8×10^{-6}	6.5×10^{-6}
TBPC-611 + BPTFSI	304	2.4×10^{18}	7.9×10^{-4}	8.8×10^{-4}
spiro-OMeTAD + BPTFSI	25	8.7×10^{17}	1.7×10^{-4}	1.9×10^{-4}

[a] μ_h^{σ} is the hole mobility derived from σ. μ_h^{SCLC} is the hole mobility derived from SCLC measurement.

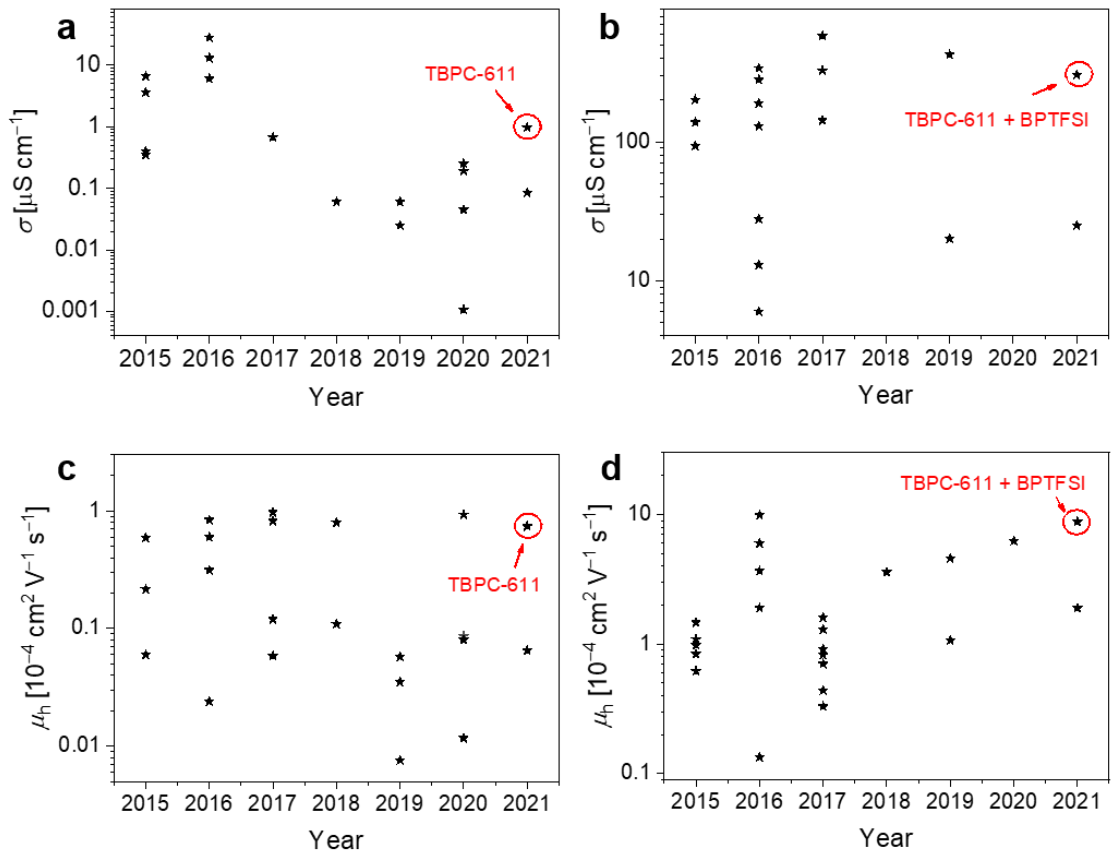

Fig. S7 (a) The σ values of neat HTMs for PSCs. It must be pointed out that a high level of unintentional doping must occur for the sample with σ larger than 1 μS cm^{-1}. (b) The σ values of doped HTMs for PSCs. (c) The μ_h values of neat HTMs for PSCs. (d) The μ_h values of doped HTMs for PSCs.

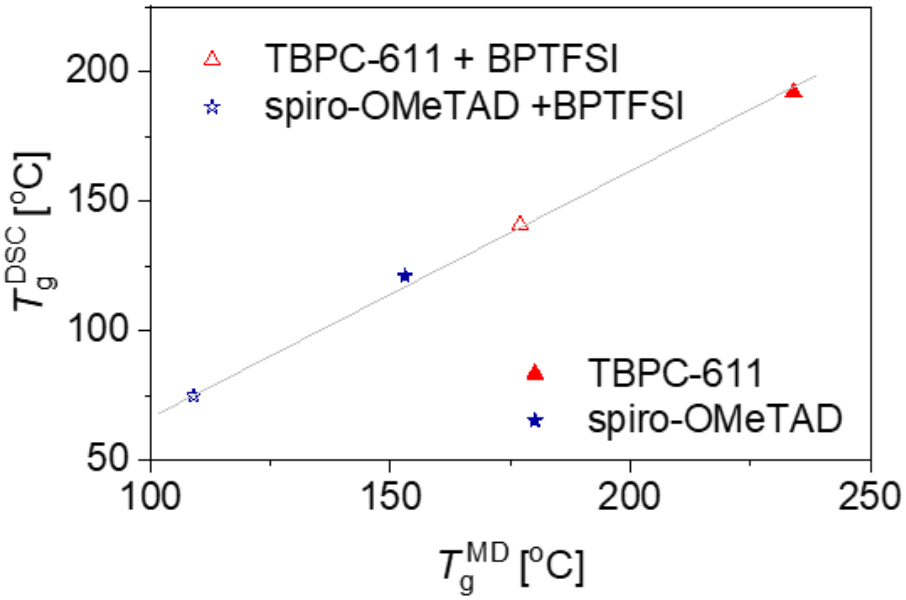

Fig. S8 The correlation between the theoretical (T_g^{MD}) and experimental (T_g^{DSC}) glass transition temperatures. The gray line is linear fitting.

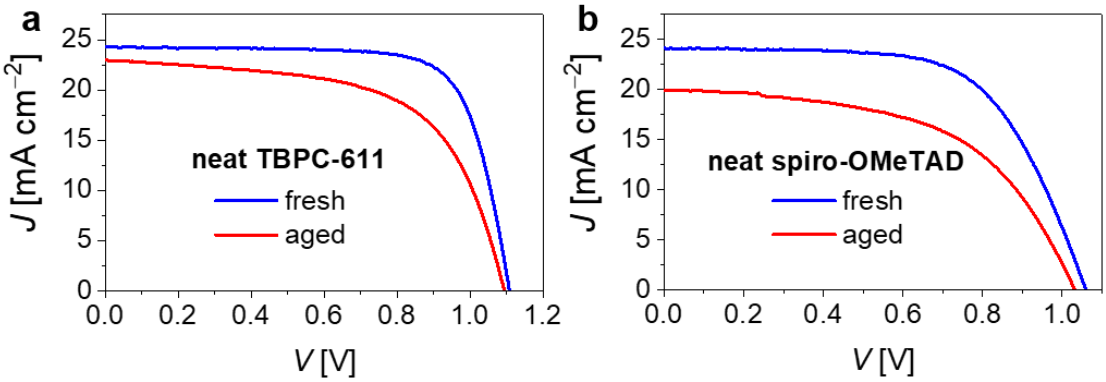

Fig. S9 The typical *J*–*V* curves of the fresh and aged PSCs with neat TBPC-611 or spiro-OMeTAD measured at the 100 mW cm^{-2}, AM1.5G conditions.

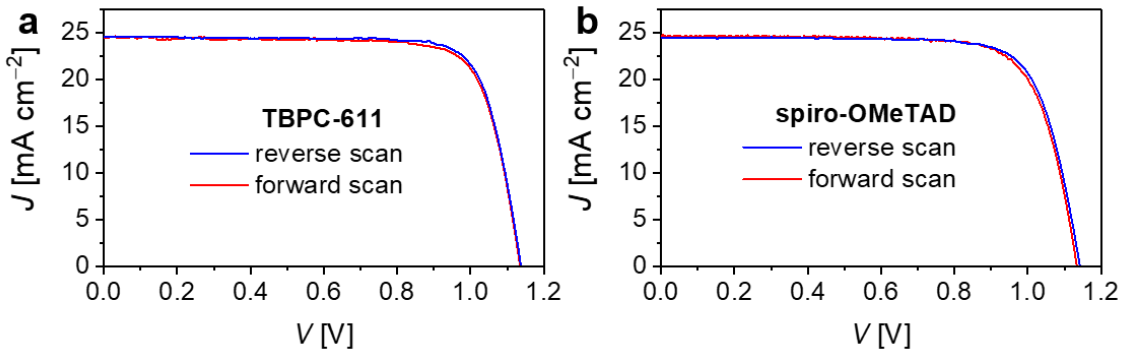

Fig. S10 The *J*–*V* curves recorded with different scan directions of a typical PSC with BPTFSI under the irradiation of 100 mW cm^{-2}, AM1.5G sunlight.

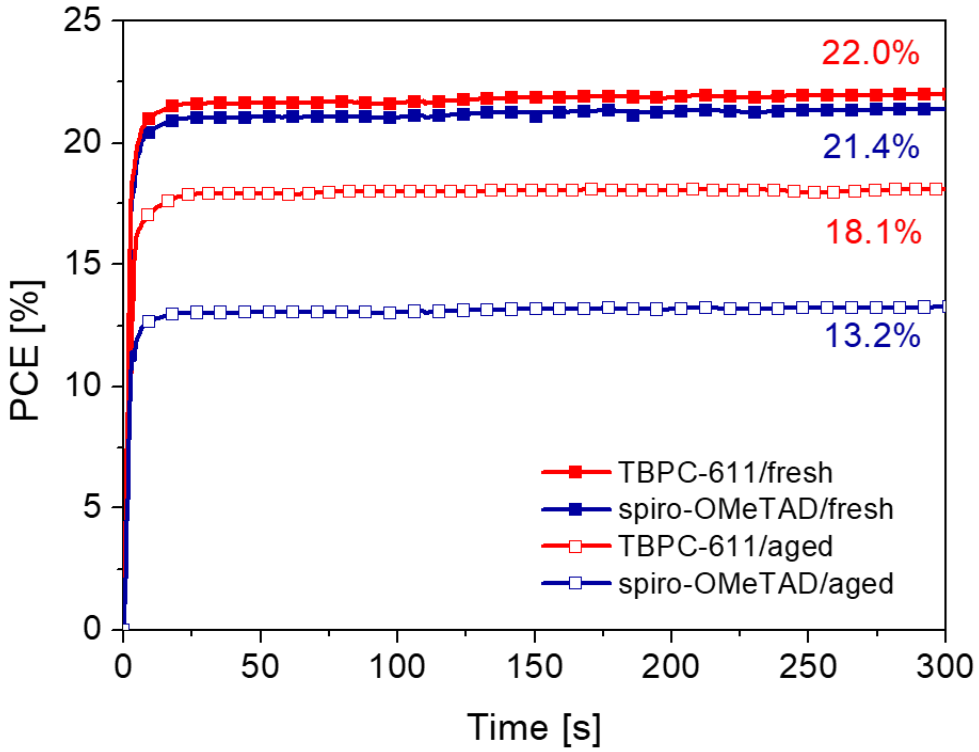

Fig. S11 The maximum power point tracking curves of the fresh and aged cells with BPTFSI. Aging was performed at 85 ºC for 2000 h.

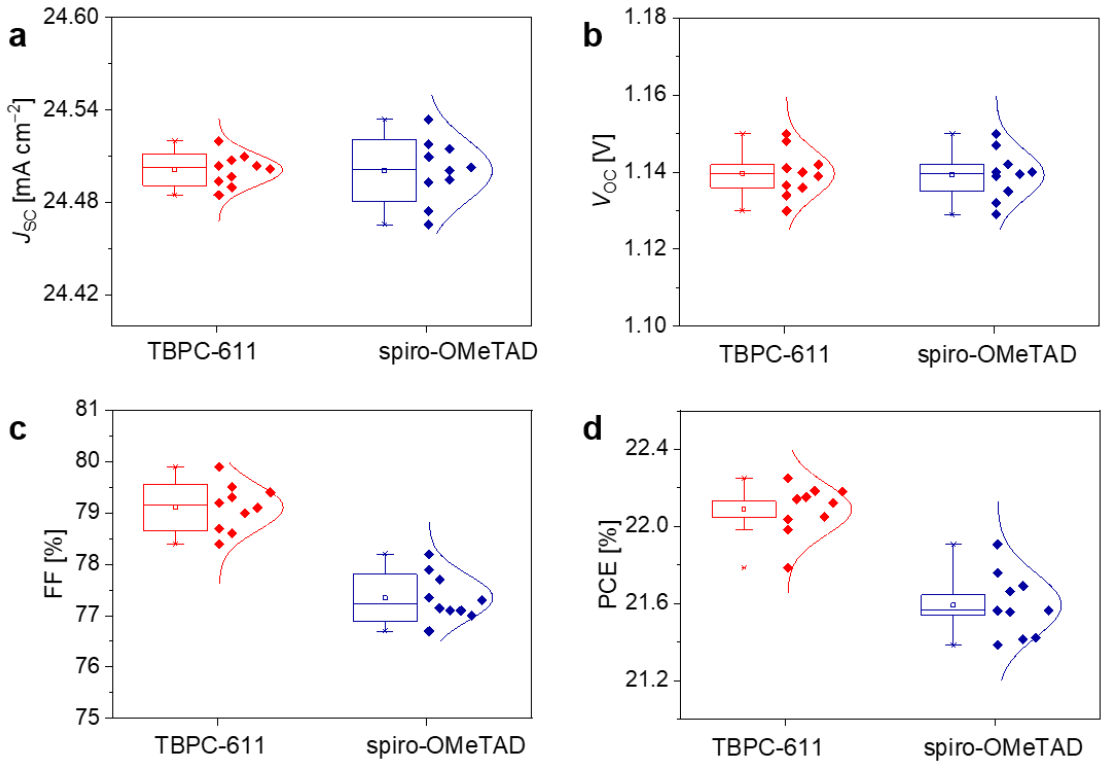

Fig. S12 The statistical analyses of photovoltaic parameters of PSCs with BPTFSI.

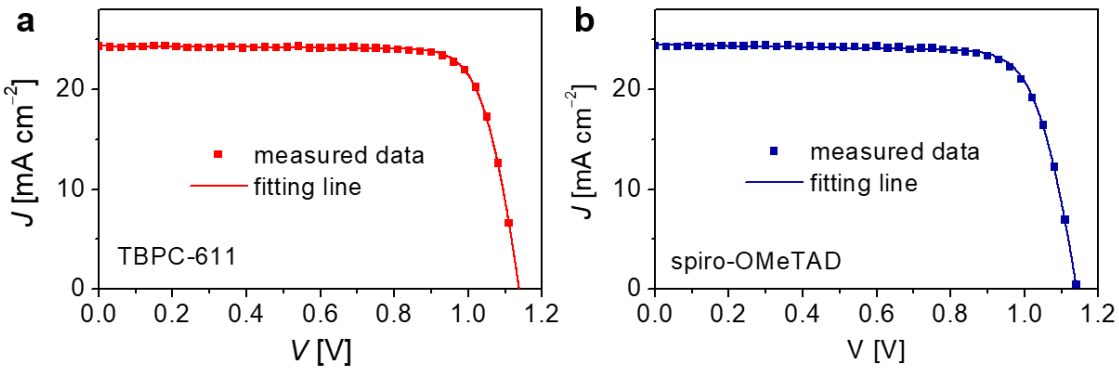

c

PSC	J_{sc} [mA cm^{-2}]	V_{oc} [V]	FF [%]	PCE [%]
TBPC-611/measured	24.5	1.140	79.1	22.1
TBPC-611/simulated	24.5	1.139	79.4	22.1
spiro-OMeTAD/measured	24.5	1.140	77.2	21.6
spiro-OMeTAD/simulated	24.5	1.139	77.7	21.6

Fig. S13 (a,b) The measured *J*–*V* data of the fresh PSCs with BPTFSI at the 100 mW cm^{-2}, AM1.5G conditions and fitting lines. (c) Comparison of the measured and simulated photovoltaic parameters.

Table S4 The typical fitting parameters of fresh and aged PSCs with BPTFSI

Device	R_{sh} [kΩ]	I_s [A]	R_s [Ω]	n
TBPC-611/fresh	19.1	3.6×10^{-15}	13.4	1.59
spiro-OMeTAD/fresh	10.1	1.4×10^{-14}	15.6	1.68
TBPC-611/aged	5.0	8.5×10^{-13}	22.5	1.95
spiro-OMeTAD/aged	2.5	2.5×10^{-11}	40.1	2.20

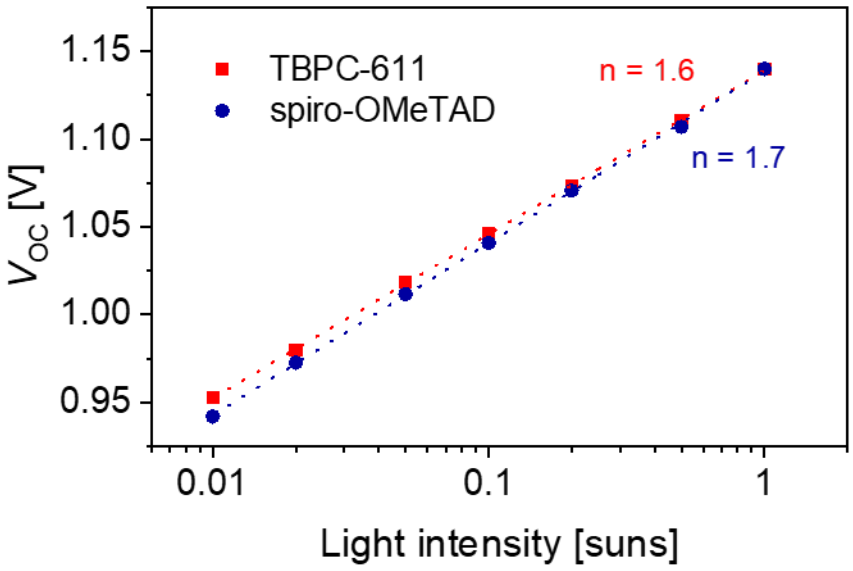

Fig. S14 The plots of V_{OC} as a function of light intensity for the fresh PSCs with BPTFSI.

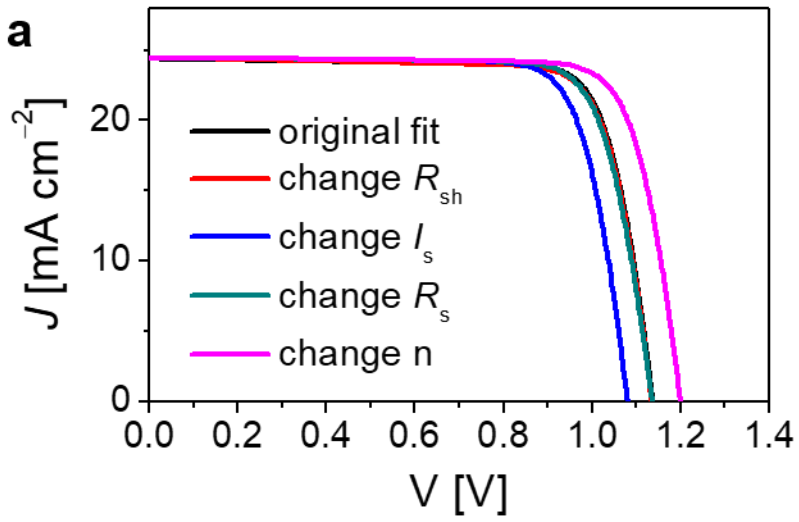

b

Substituted parameter	R_{sh} [kΩ]	I_s [A]	R_s [Ω]	n	J_{SC} [mA cm^{-2}]	V_{OC} [V]	FF [%]	PCE [%]
/	19.1	3.6×10^{-15}	13.4	1.59	24.5	1.139	79.4	22.1
R_{sh}	10.1	3.6×10^{-15}	13.4	1.59	24.5	1.136	78.8	21.9
I_s	19.1	1.4×10^{-14}	13.4	1.59	24.5	1.080	78.9	20.8
R_s	19.1	3.6×10^{-15}	15.6	1.59	24.5	1.139	78.7	21.9
n	19.1	3.6×10^{-15}	13.4	1.68	24.5	1.200	79.6	23.4

Fig. S15 (a) The simulated *J*–*V* curves by using one physical parameter of the fresh spiro-OMeTAD cell in combination with the other four physical parameters of the fresh TBPC-611 cell. (b) The Simulated *J*–*V* curves and related photovoltaic parameters. By using one physical parameter (marked in red) of the fresh spiro-OMeTAD cell in combination with the other four physical parameters (marked in blue) of the fresh TBPC-611 cell, we numerically simulated a new *J*–*V* curve with a new set of photovoltaic parameters. The photovoltaic parameters and simulated physical parameters of the fresh TBPC-611 cell are listed in the second row.

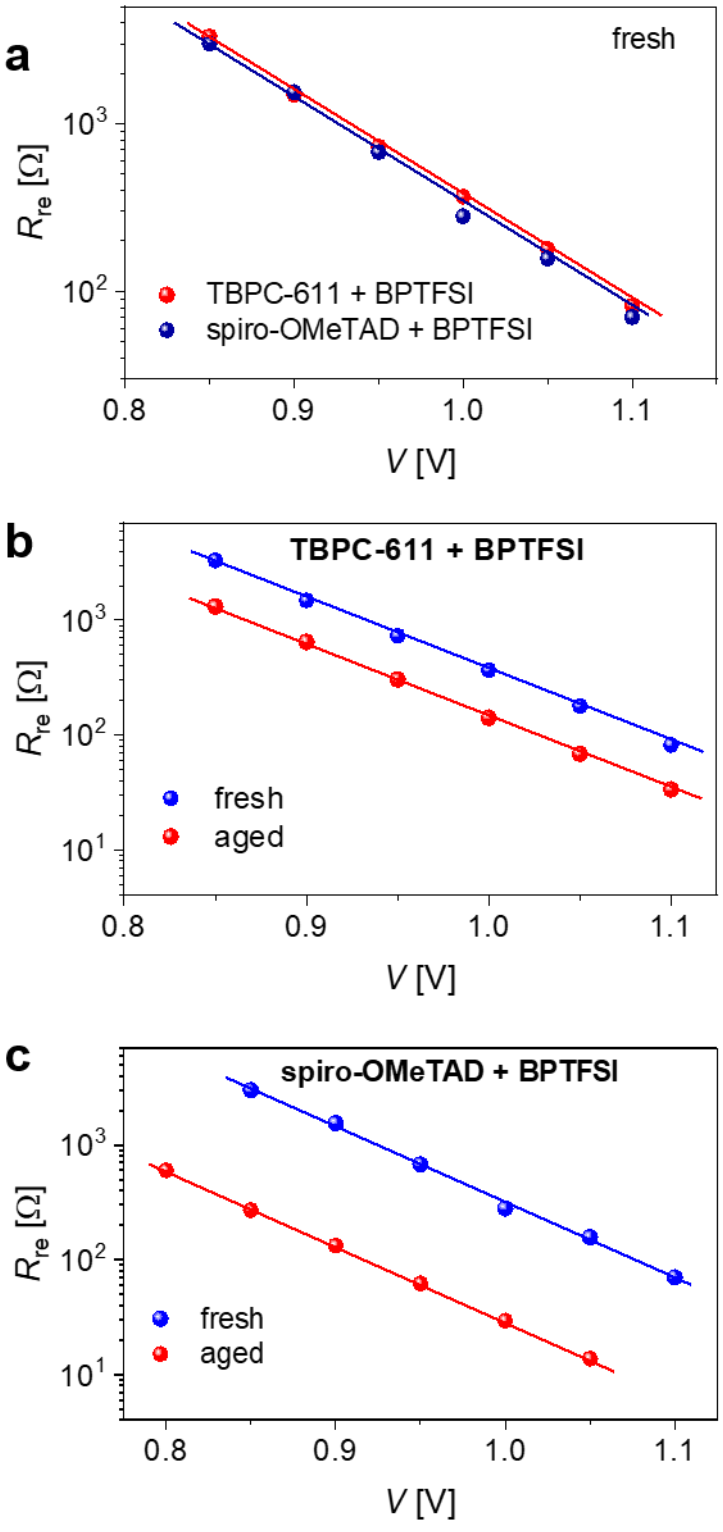

Fig. S16 Plots of charge recombination resistance (R_{re}) as a function of bias potential (V) for PSCs with BPTFSI. The lines are drawn as a guide to the eyes.

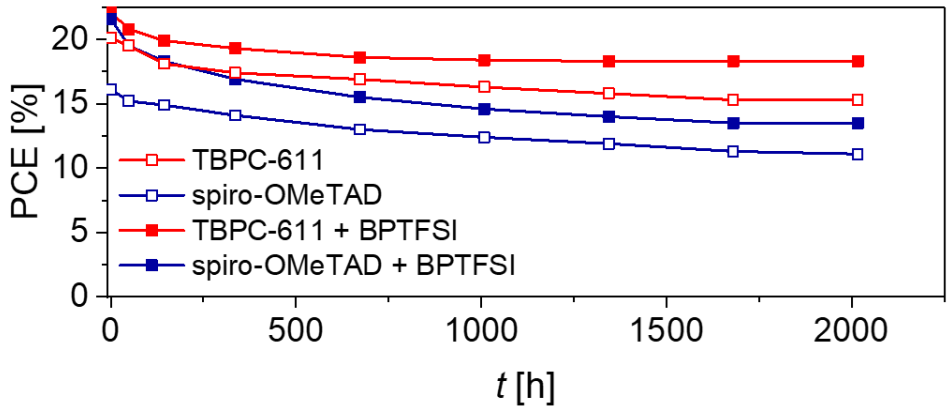

Fig. S17 The PCE evolution of the sealed PSCs stored at 85 °C with 45–90% environment humidity.

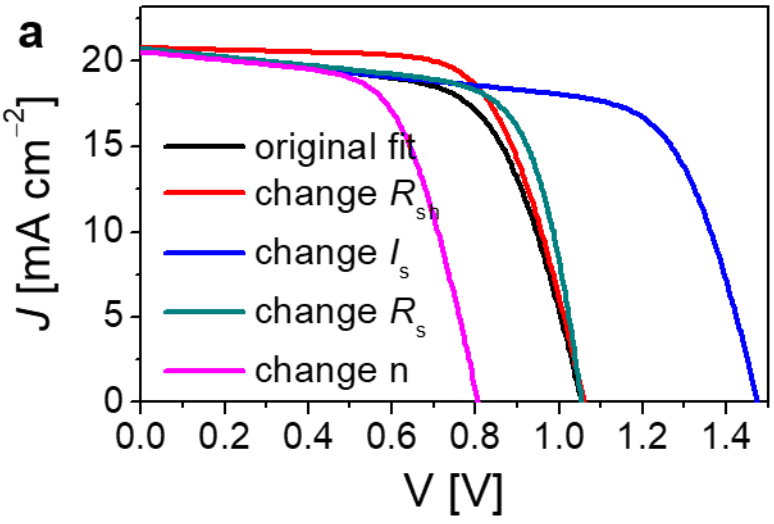

b

Substituted parameter	R_{sh} [kΩ]	I_s [A]	R_s [Ω]	n	J_{SC} [mA cm^{-2}]	V_{OC} [V]	FF [%]	PCE [%]
/	2.5	2.5×10^{-11}	40.1	2.20	20.5	1.064	62.2	13.6
R_{sh}	10.1	2.5×10^{-11}	40.1	2.20	20.8	1.068	67.1	14.9
I_s	2.5	1.4×10^{-14}	40.1	2.20	20.6	1.470	66.5	20.1
R_s	2.5	2.5×10^{-11}	15.6	2.20	20.8	1.064	69.3	15.3
n	2.5	2.5×10^{-11}	40.1	1.68	20.6	0.806	62.2	10.3

Fig. S18 (a) The simulated *J*–*V* curves by using one physical parameter of the fresh spiro-OMeTAD cell in combination with the other four physical parameters of the aged spiro-OMeTAD cell. (b) The Simulated *J*–*V* curves and related photovoltaic parameters. By using one physical parameter (marked in red) of the fresh spiro-OMeTAD cell in combination with the other four physical parameters (marked in blue) of the aged spiro-OMeTAD cell, we numerically simulated a new *J*–*V* curve with a new set of photovoltaic parameters. The photovoltaic parameters and simulated physical parameters (marked in black) of the aged spiro-OMeTAD cell are listed in the second row.

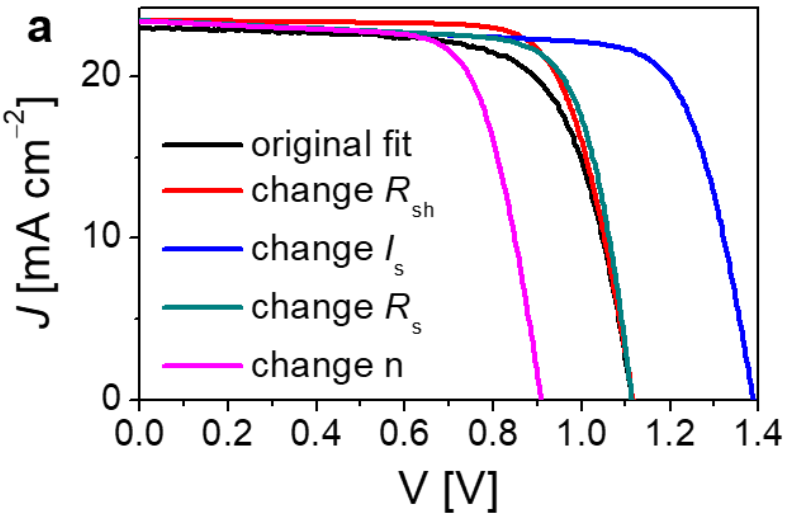

b

Substituted parameter	R_{sh} [kΩ]	I_s [A]	R_s [Ω]	n	J_{SC} [mA cm^{-2}]	V_{OC} [V]	FF [%]	PCE [%]
/	5.0	8.5×10^{-13}	22.5	1.95	23.4	1.113	70.8	18.5
R_{sh}	19.2	8.5×10^{-13}	22.5	1.95	23.5	1.117	74.4	19.5
I_s	5.0	3.6×10^{-15}	22.5	1.95	23.4	1.388	74.7	24.2
R_s	5.0	8.5×10^{-13}	13.4	1.95	23.4	1.113	74.9	19.5
n	5.0	8.5×10^{-13}	22.5	1.59	23.4	0.909	71.4	15.2

Fig. S19 (a) The simulated *J*–*V* curves by using one physical parameter of the fresh TBPC-611 cell in combination with the other four physical parameters of the aged TBPC-611 cell. (b) The simulated *J*–*V* curves and related photovoltaic parameters. By using one physical parameter (marked in red) of the fresh TBPC-611 cell in combination with the other four physical parameters (marked in blue) of the aged TBPC-611 cell, we numerically simulated a new *J*–*V* curve with a new set of photovoltaic parameters. The photovoltaic parameters and simulated physical parameters of the aged TBPC-611 cell are listed in the second row.

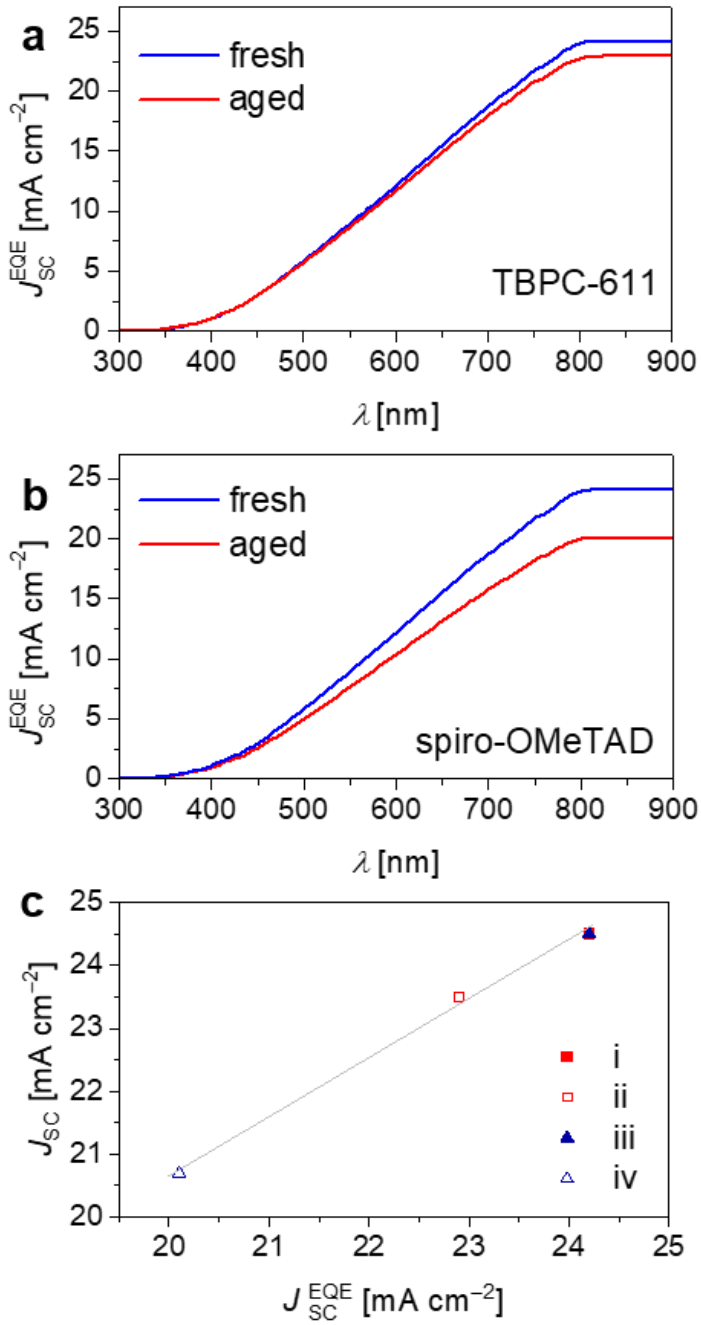

Fig. S20 (a,b) Photocurrent densities (J_{SC}^{EQE}) predicted from the integral of the product of EQE and the photo flux of the AM1.5G emission spectrum (ASTM G173-03) over the wavelength, for fresh and aged PSCs with BPTFSI. (c) Correlation between J_{SC}^{EQE} and J_{SC} for (i) the fresh PSC with TBPC-611, (ii) the aged PSC with TBPC-611, (iii) the fresh PSC with spiro-OMeTAD, and (iv) the aged PSC with spiro-OMeTAD. The gray line is the linear fitting.

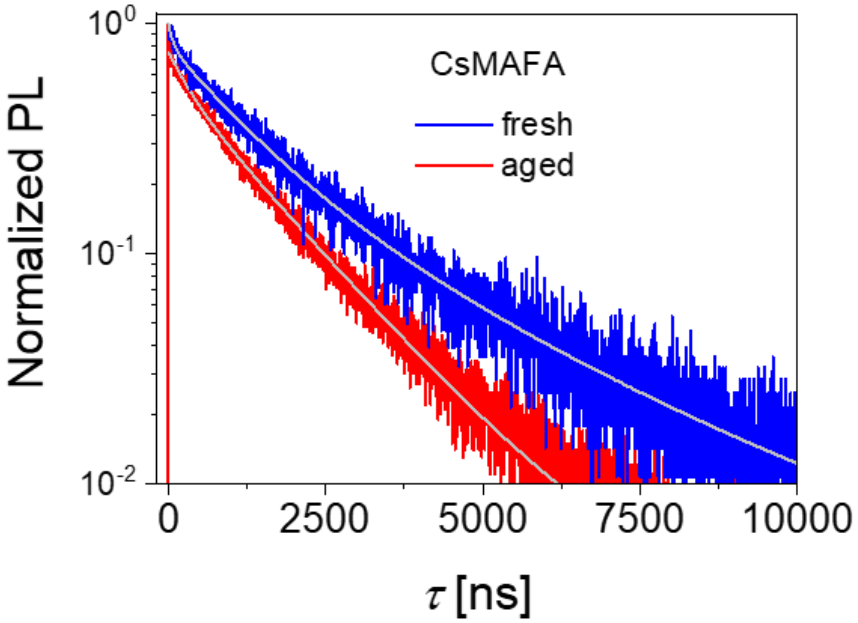

Fig. S21 The TRPL traces of the PVK-coated CsMAFA on the alumina substrate before and after 2000 h, 85 ºC aging. Double-exponential fittings are shown as gray lines.

Table S5 The fitting parameters of TRPL decays and charge separation yields[a]

Sample	τ_1 [ns]	A_1	τ_2 [ns]	A_2	$\bar{\tau}$ [ns]	ϕ_{cs} [%]
Al_2O_3/CsMAFA/PVK/fresh	224	0.27	1641	0.73	1258	/
Al_2O_3/CsMAFA/PVK/aged	272	0.27	1104	0.73	879	/
TiO_2/CsMAFA/TBPC-611/fresh	3	0.79	47	0.21	12	99.1
TiO_2/CsMAFA/TBPC-611/aged	7	0.72	37	0.28	15	98.3
TiO_2/CsMAFA/spiro-OMeTAD/fresh	6	0.74	62	0.26	20	98.4
TiO_2/CsMAFA/spiro-OMeTAD/fresh	11	0.56	67	0.44	36	95.9

[a] τ_1 and τ_2 are the time constants of fast and slow decays, A_1 and A_2 are the relative amplitudes of fast and slow decays, and $\bar{\tau}$ is the amplitude-averaged time constant which is calculated by equation $\bar{\tau} = A_1\tau_1 + A_2\tau_2$. ϕ_{cs} is the yield of charge seperation derived with equaltion $\phi_{cs} = \frac{\bar{\tau}_{PVK} - \bar{\tau}_{HTL}}{\bar{\tau}_{PVK}}$, where $\bar{\tau}_{PVK}$ is the amplitude-averaged time constant of the PVK-covered CsMAFA on the alumina substrate, and $\bar{\tau}_{HTL}$ is the amplitude-averaged time constant of HTL-covered CsMAFA on the titania substrate.

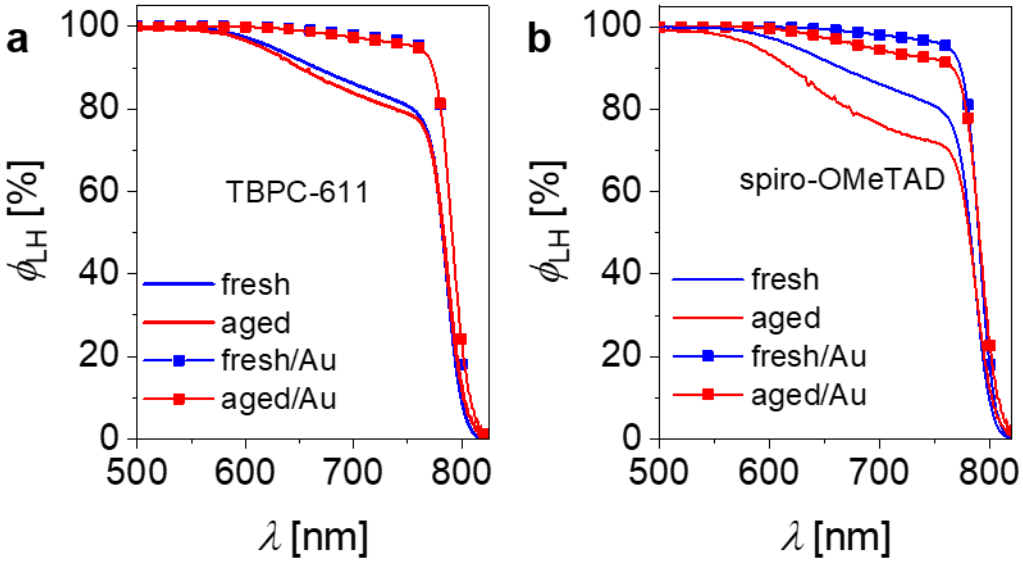

Fig. S22 Plots of light-harvesting yield (ϕ_{LH}) as a function of wavelength. Assuming the gold electrode has the effect of total reflection, we deduced the improved ϕ_{LH} values (line + symbol).

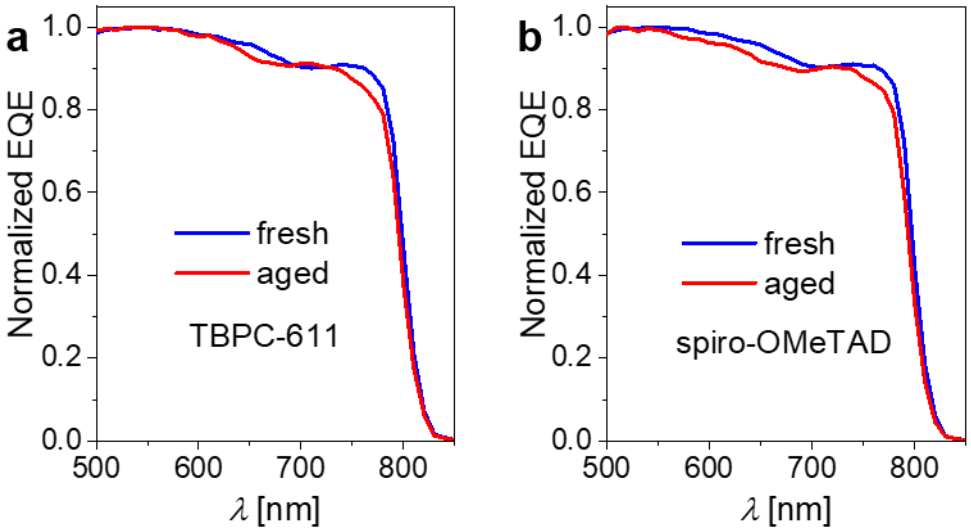

Fig. S23 The normalized EQE spectra of the fresh and aged PSCs with BPTFSI.

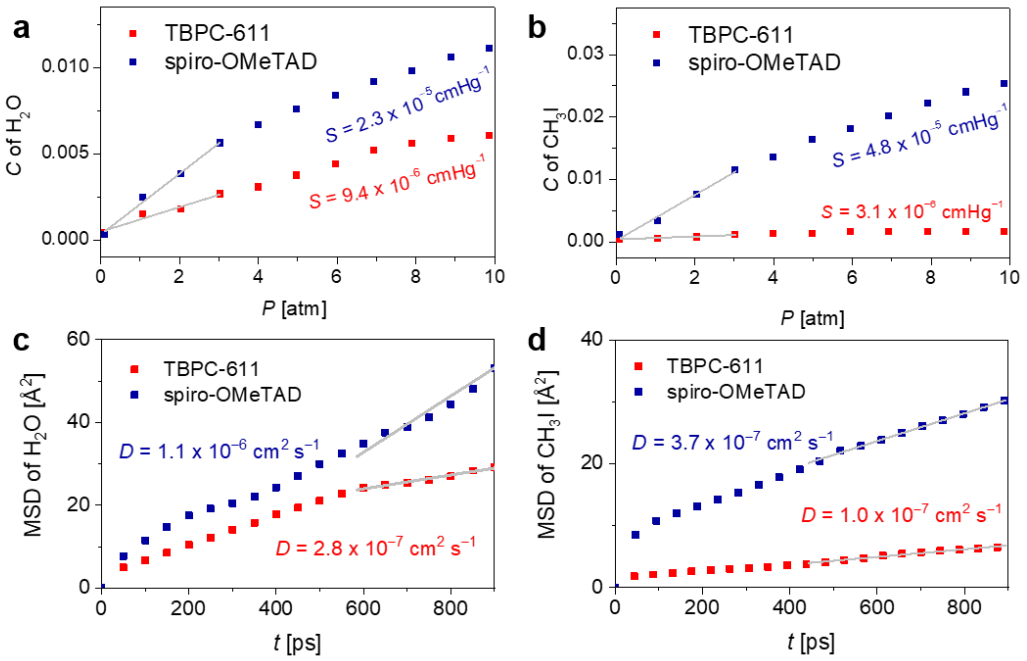

Fig. S24 (a,b) The adsorption isotherms of H_2O and CH_3I in the 15% BPTFSI-containing composites at 85 °C. From the limiting slope when pressure is zero, the solubility coefficient (S) is derived. (c,d) The mean square displacements (MSD) of H_2O and CH_3I in the BPTFSI composites at 85 °C. From the linear fitting of MSD within 600−1000 ps, the diffusion coefficient (D) is obtained.

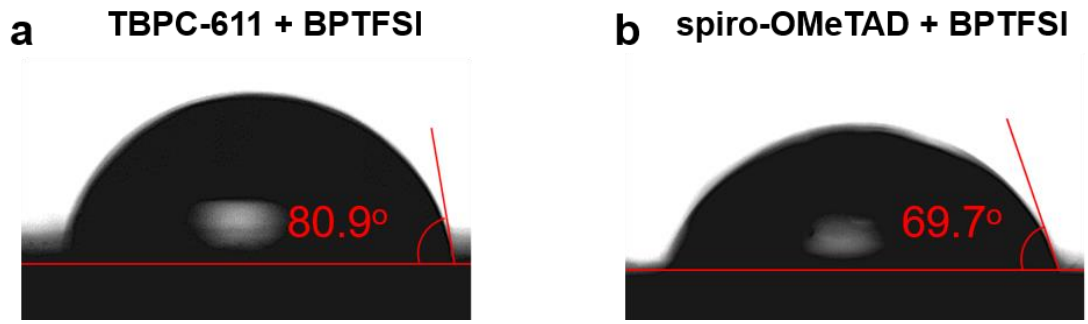

Fig. S25 The water contact angles of the BPTFSI containing composite films of (a) TBPC-611 and (b) spiro-OMeTAD.

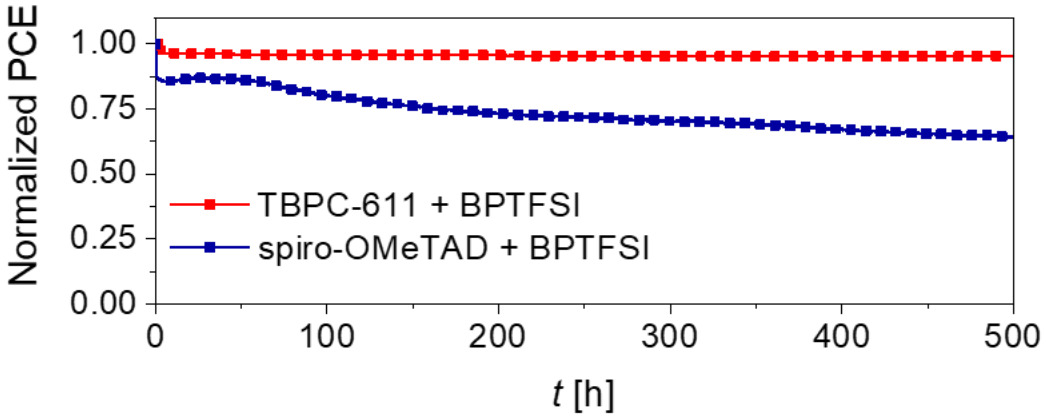

Fig. S26 The PCE evolution of PSCs with BPTFSI at 55 °C via MPP tracking under the irradiation of continuous AM 1.5G equivalent light-emitting diode array.

5. Appendix: ^{1}H NMR Spectra, ^{13}C NMR Spectra, Mass Spectra, and Infrared Spectra

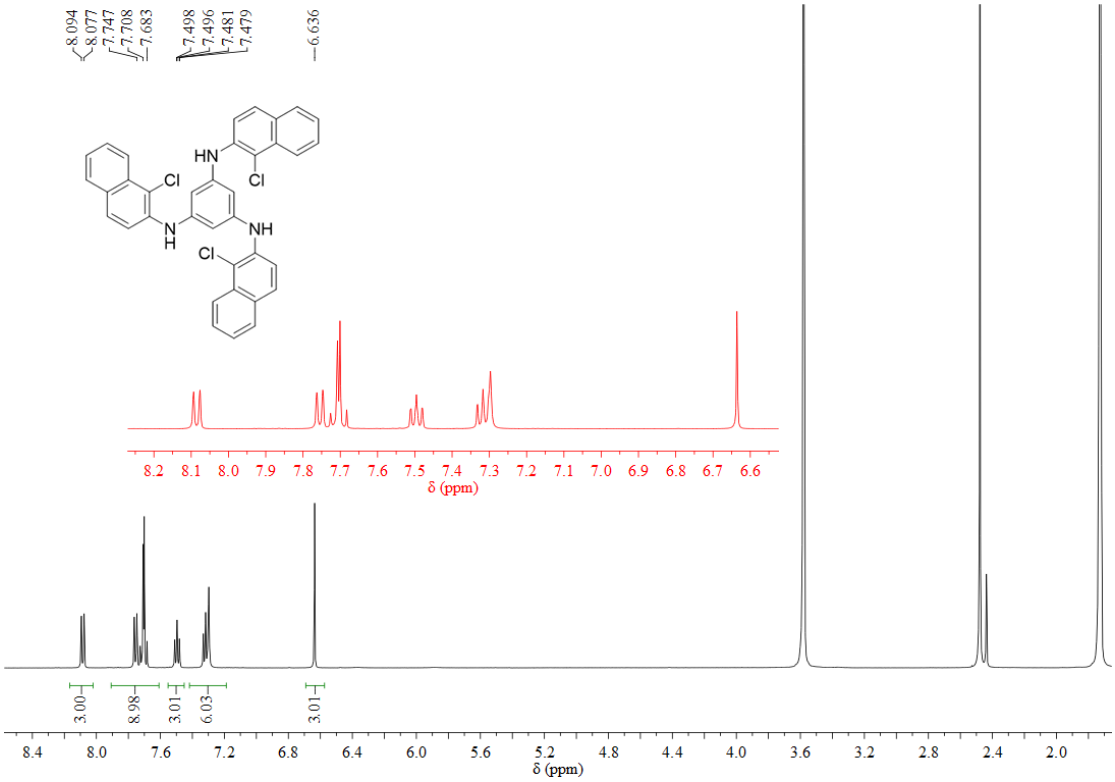

Fig. S27 The ^{1}H NMR (500 MHz) spectrum of 2 in THF-d_8.

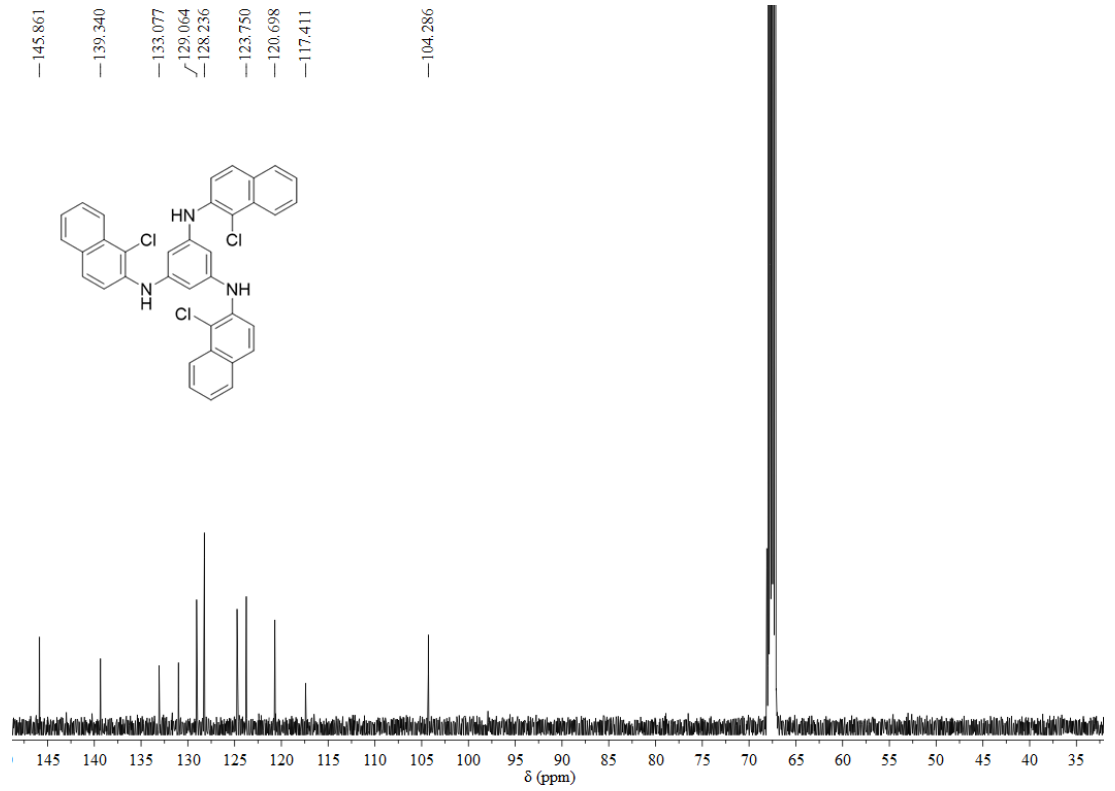

Fig. S28 The ^{13}C NMR (125 MHz) spectrum of 2 in THF-d_8.

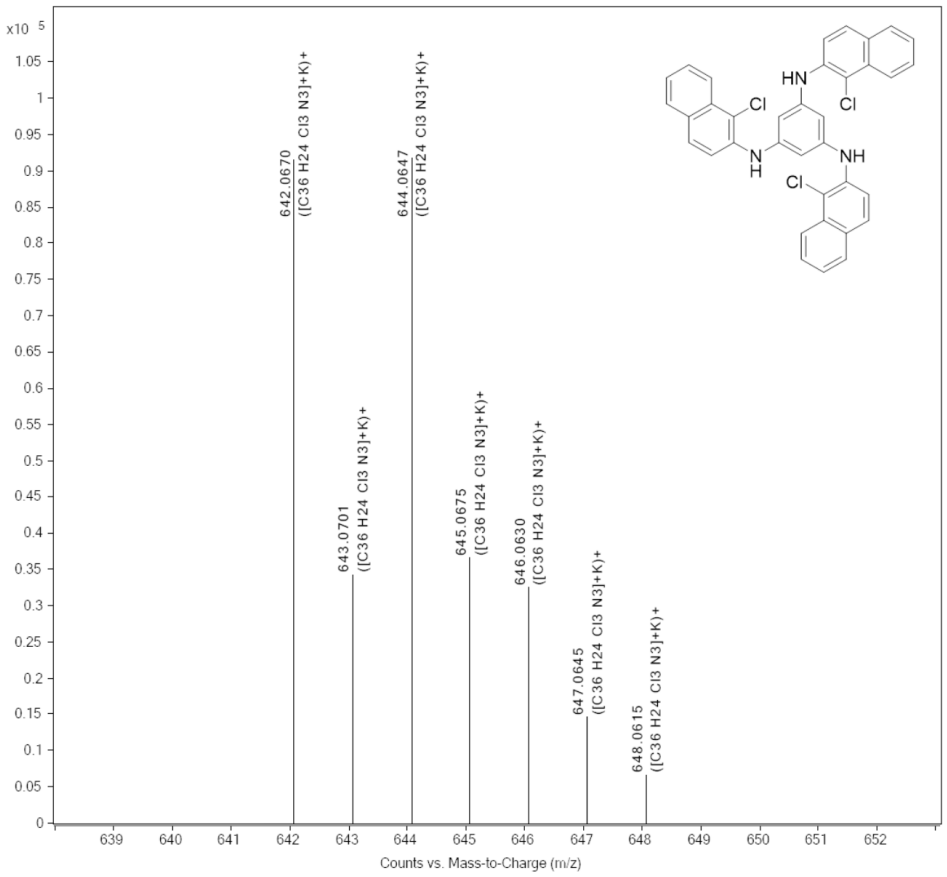

Fig. S29 The high-resolution mass spectrum (ESI) of 2.

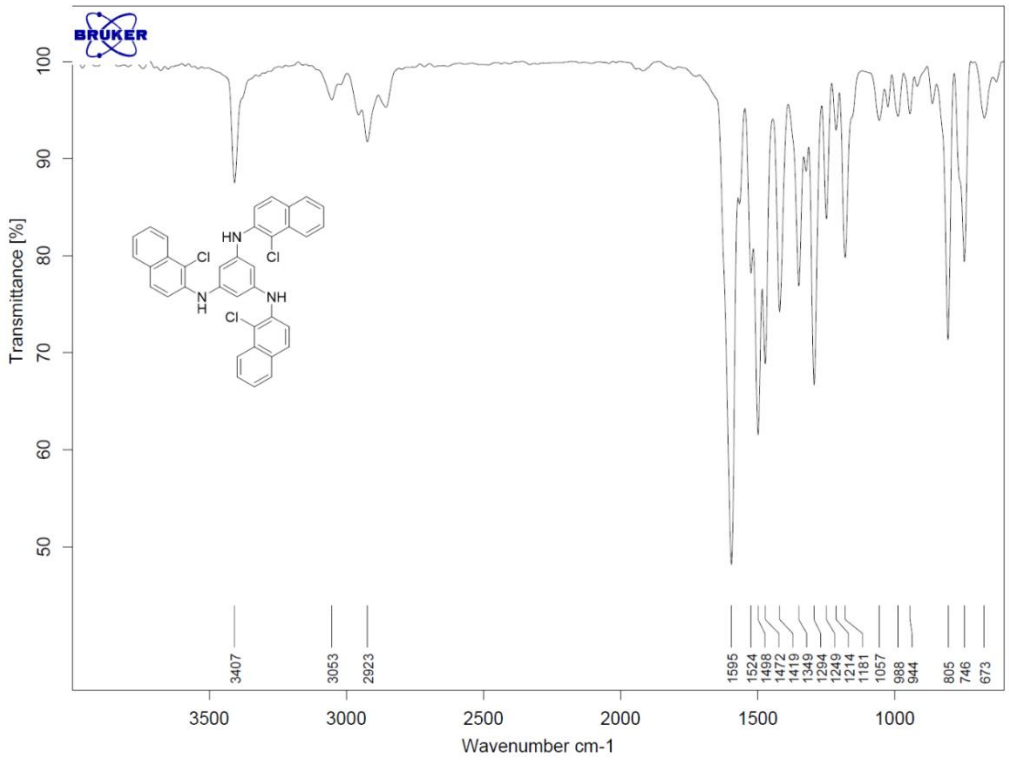

Fig. S30 The infrared spectrum of 2.

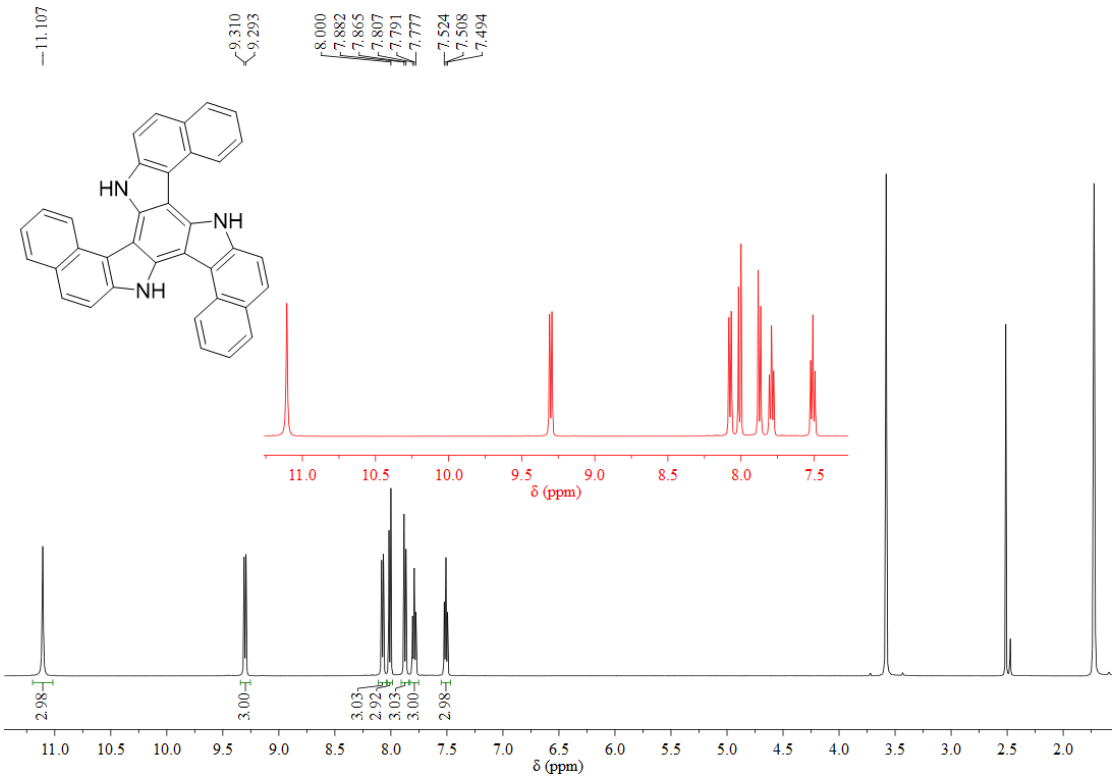

Fig. S31 The ^{1}H NMR (400 MHz) spectrum of 3 in THF-d_8.

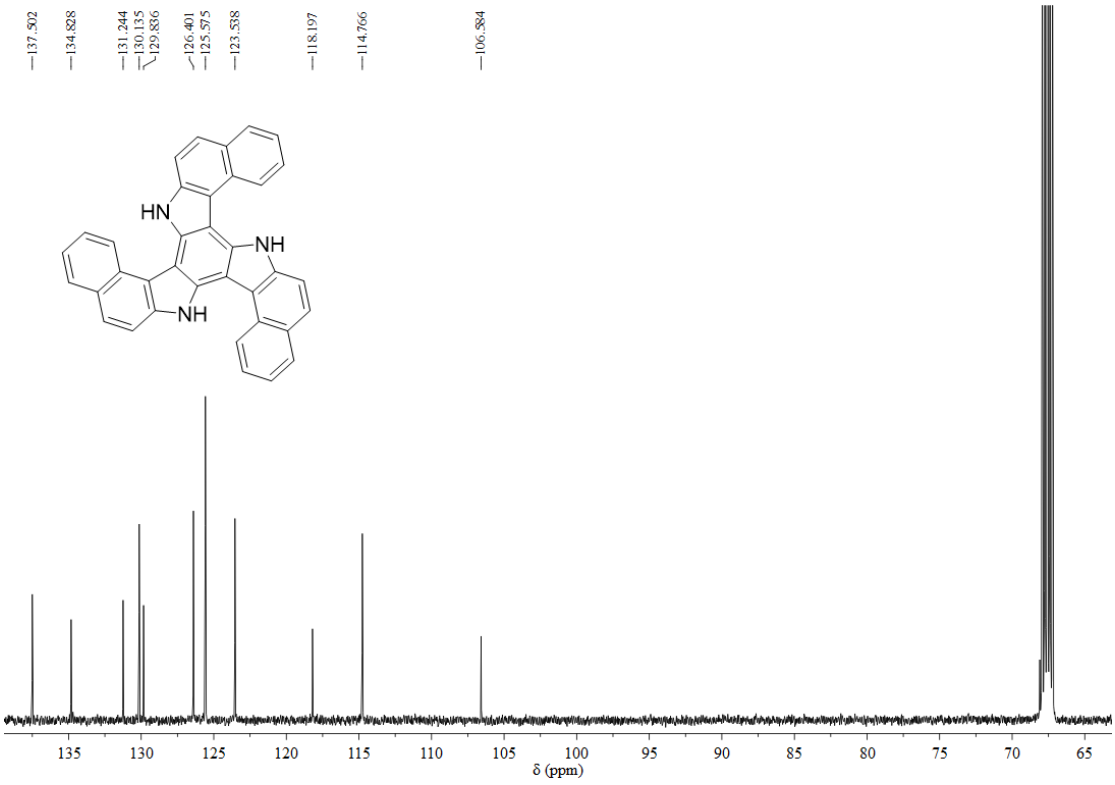

Fig. S32 The ^{13}C NMR (100 MHz) spectrum of 3 in THF-d_8.

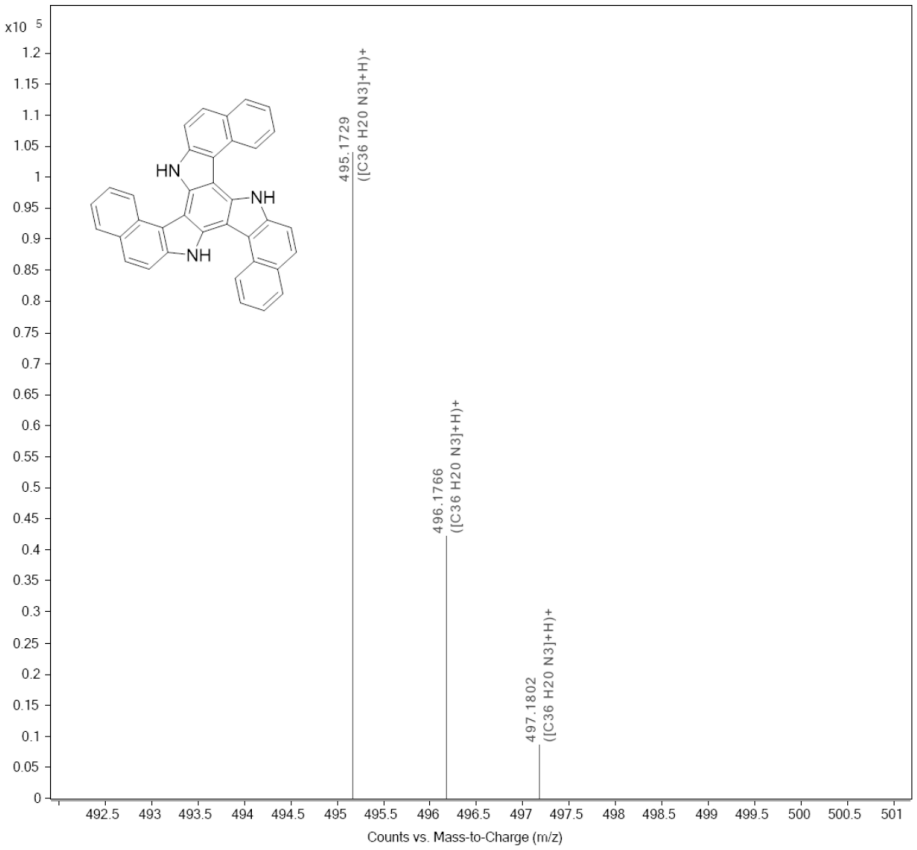

Fig. S33 The high-resolution mass spectrum (ESI) of 3.

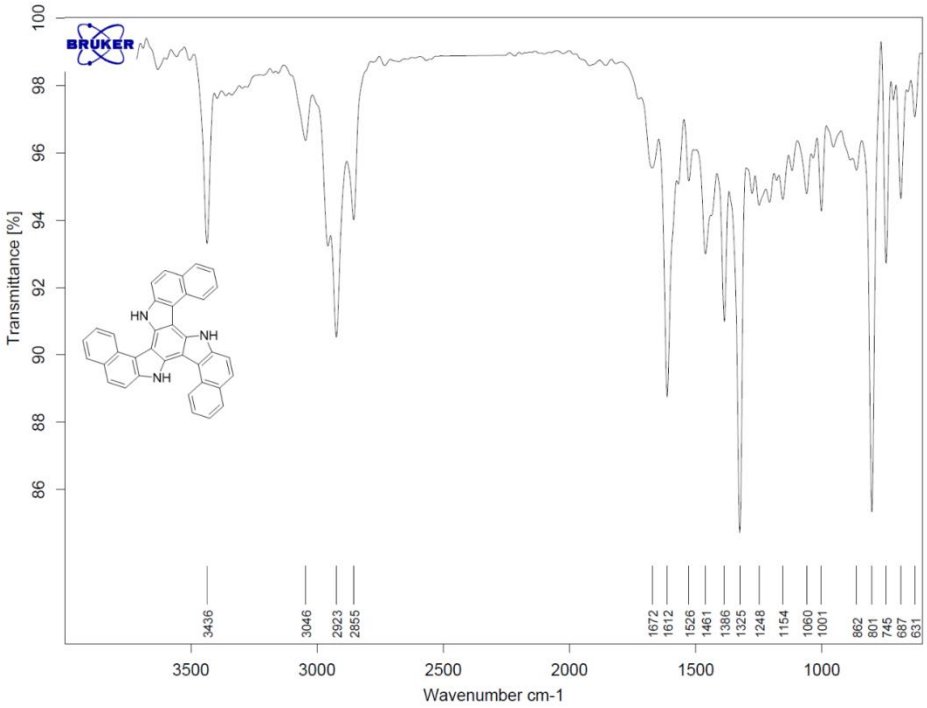

Fig. S34 The infrared spectrum of 3.

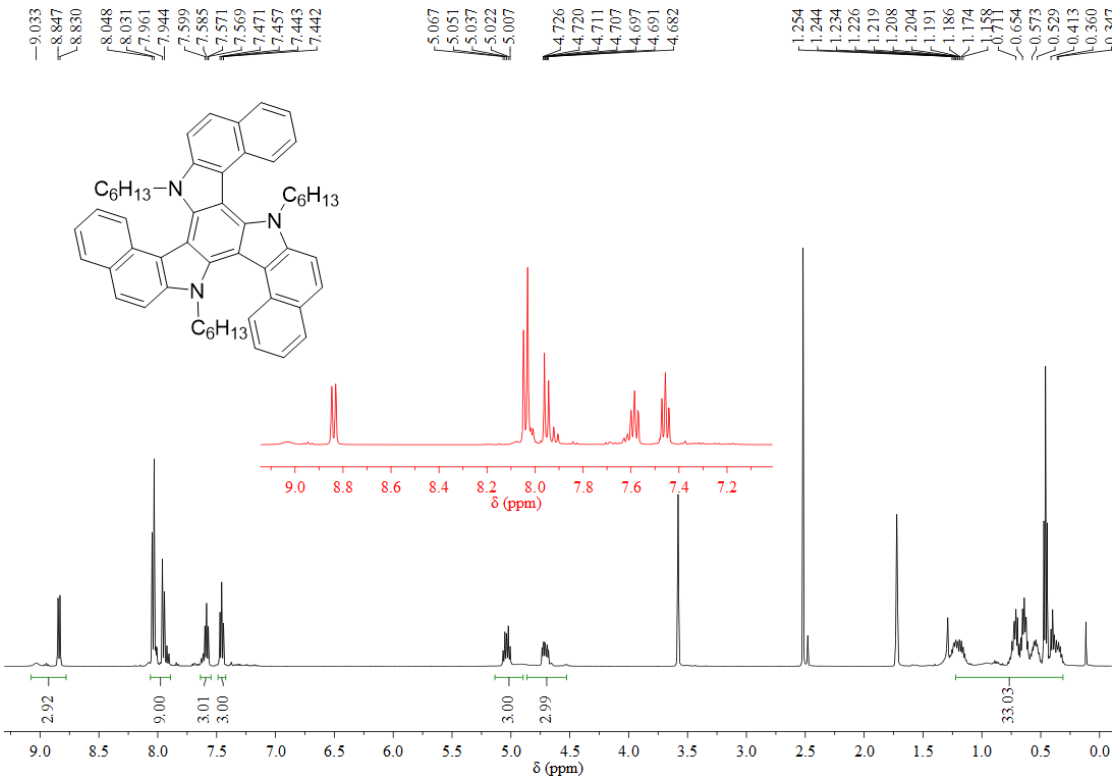

Fig. S35 The ^{1}H NMR (500 MHz) spectrum of 4 in THF-d_8.

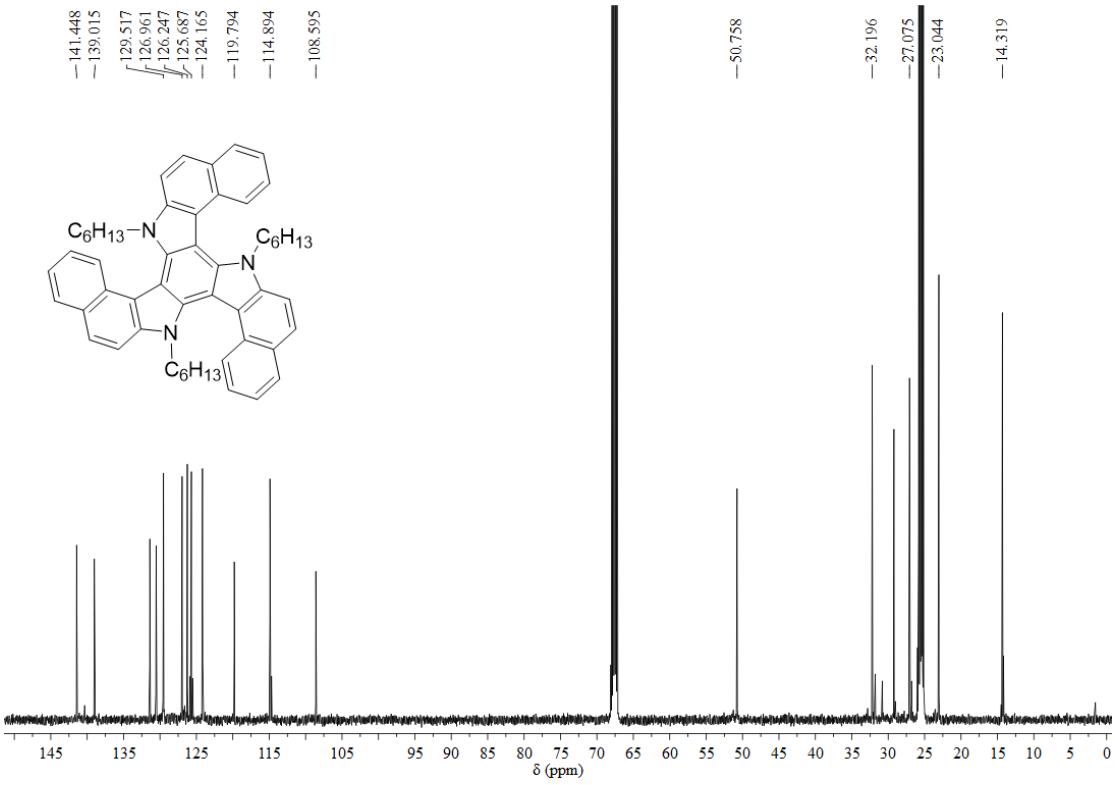

Fig. S36 The ^{13}C NMR (125 MHz) spectrum of 4 in THF-d_8.

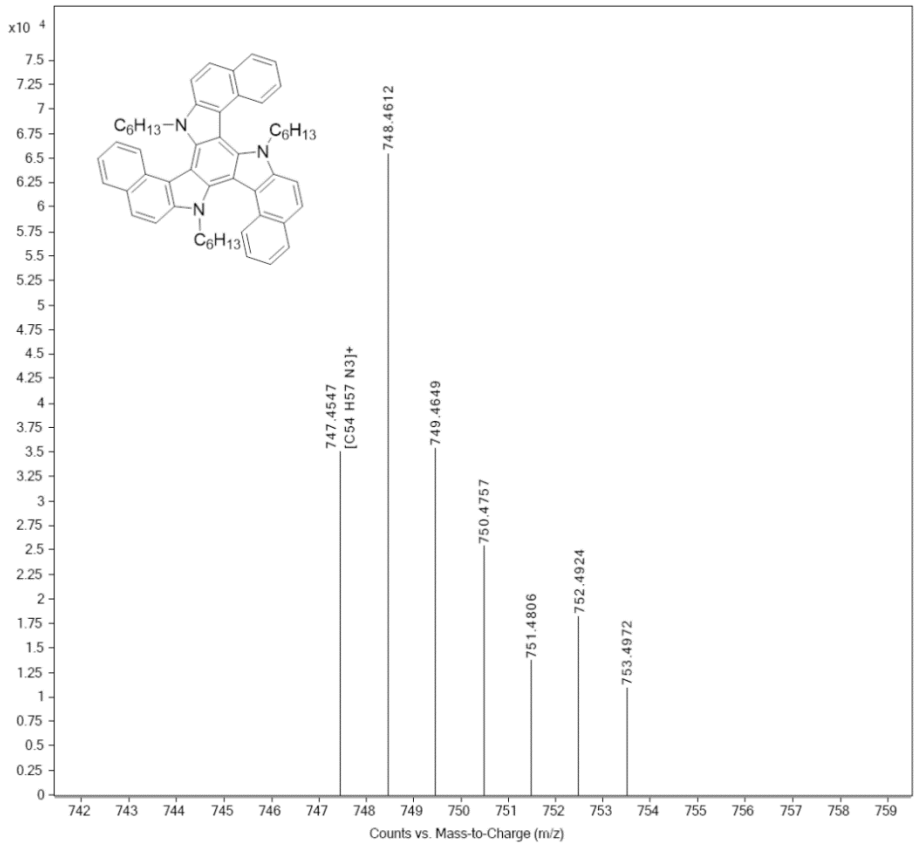

Fig. S37 The high-resolution mass spectrum (ESI) of 4.

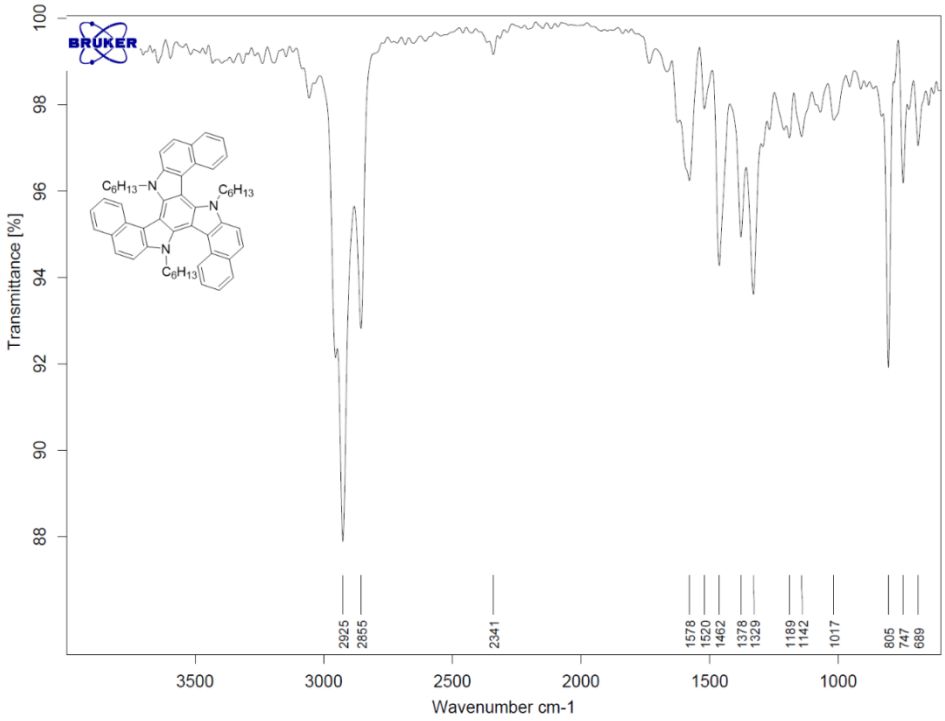

Fig. S38 The infrared spectrum of 4.

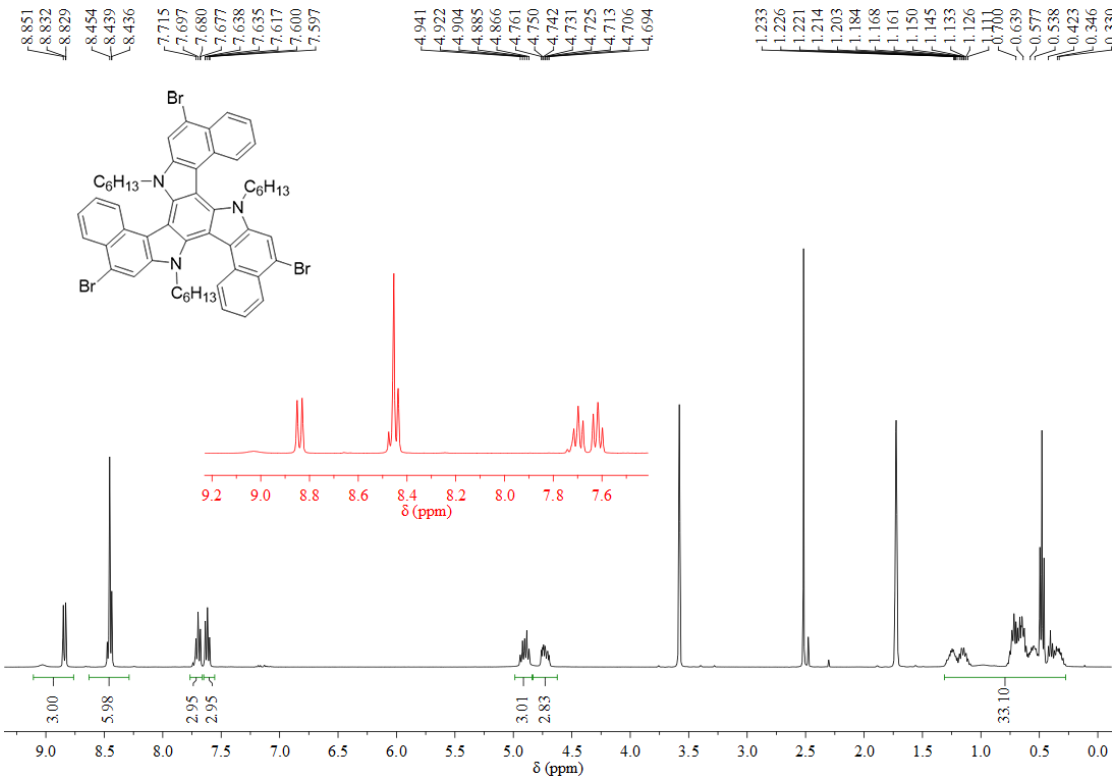

Fig. S39 The ^{1}H NMR (400 MHz) spectrum of 5 in THF-d_8.

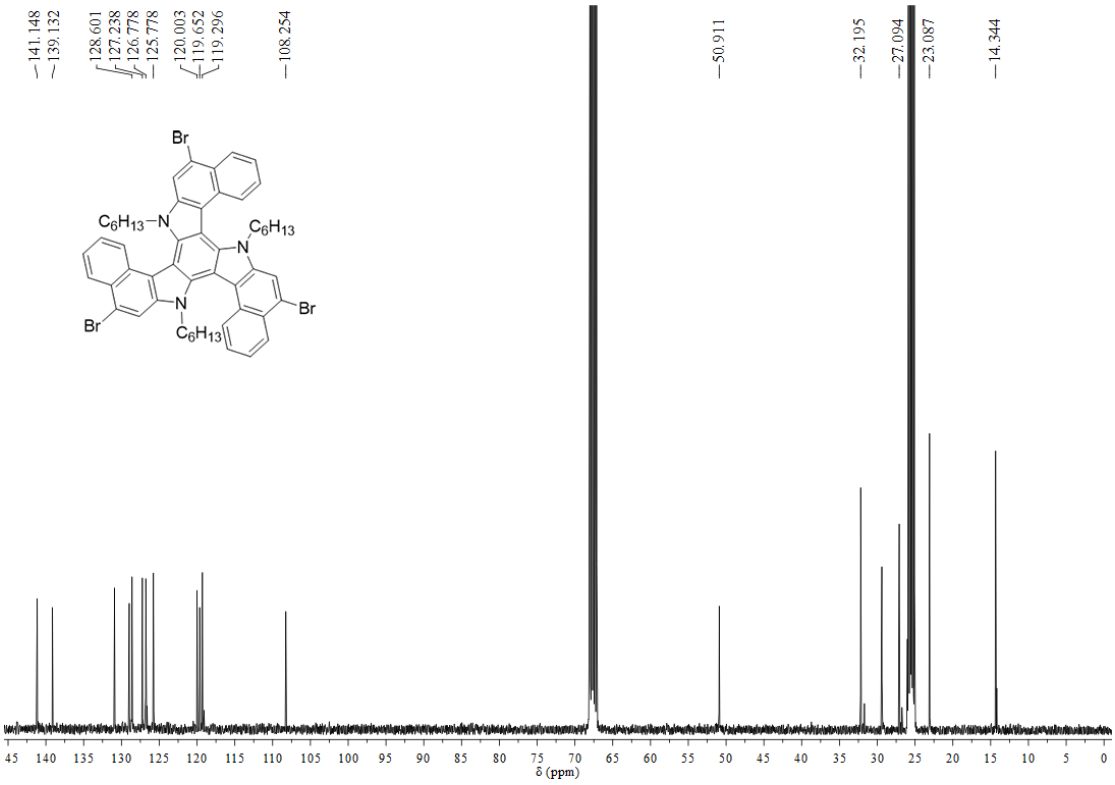

Fig. S40 The ^{13}C NMR (100 MHz) spectrum of 5 in THF-d_8.

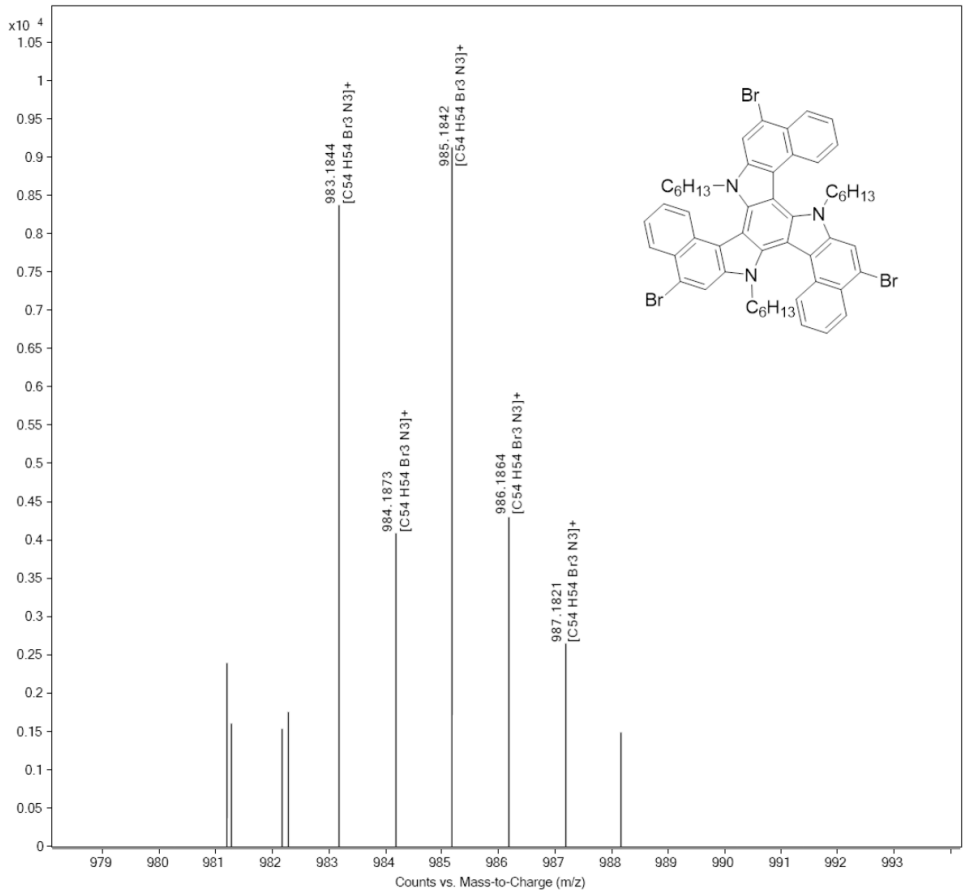

Fig. S41 The high-resolution mass spectrum (ESI) of 5.

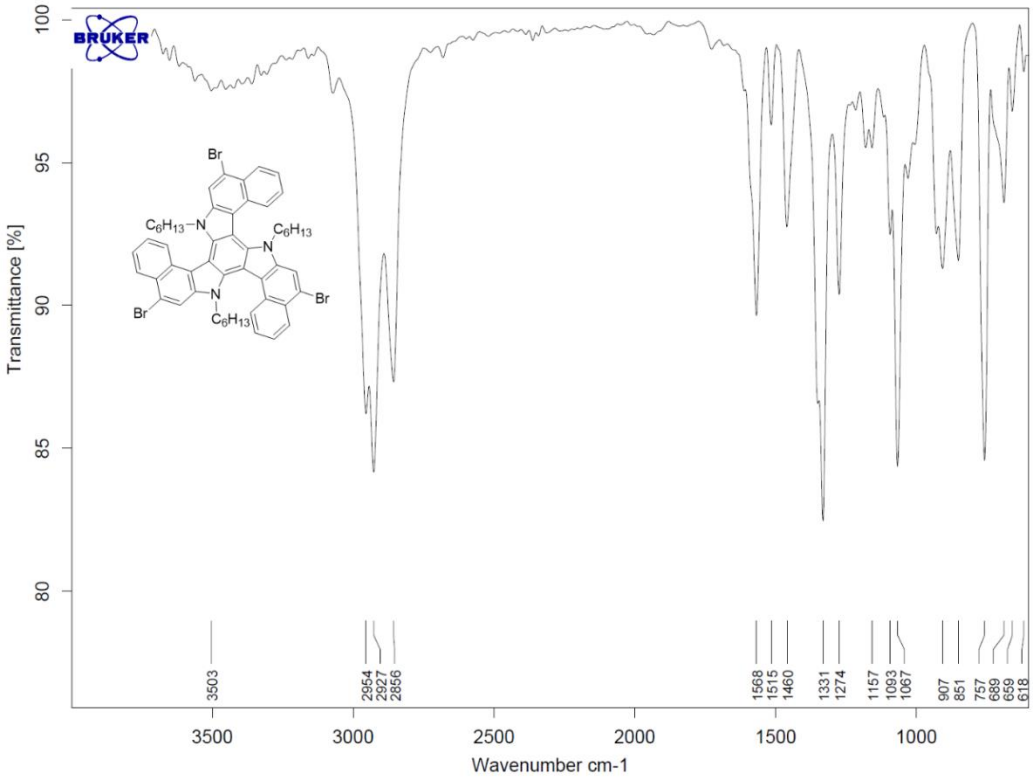

Fig. S42 The infrared spectrum of 5.

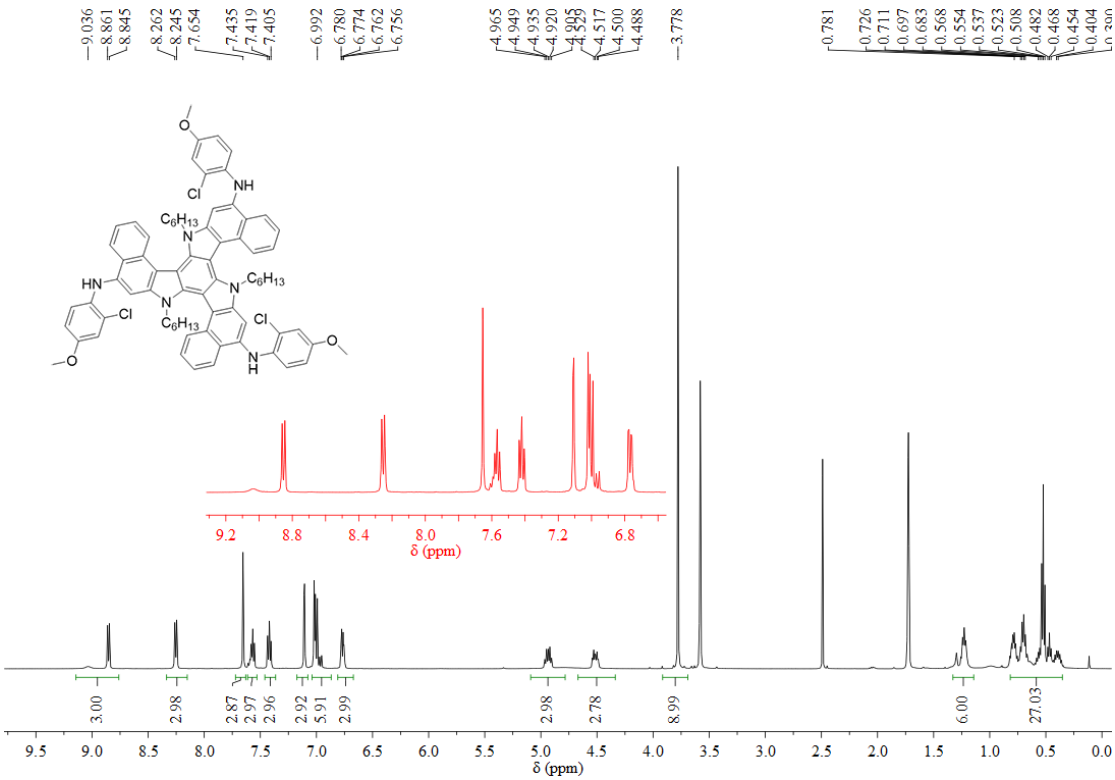

Fig. S43 The ^{1}H NMR (500 MHz) spectrum of 6 in THF-d_8.

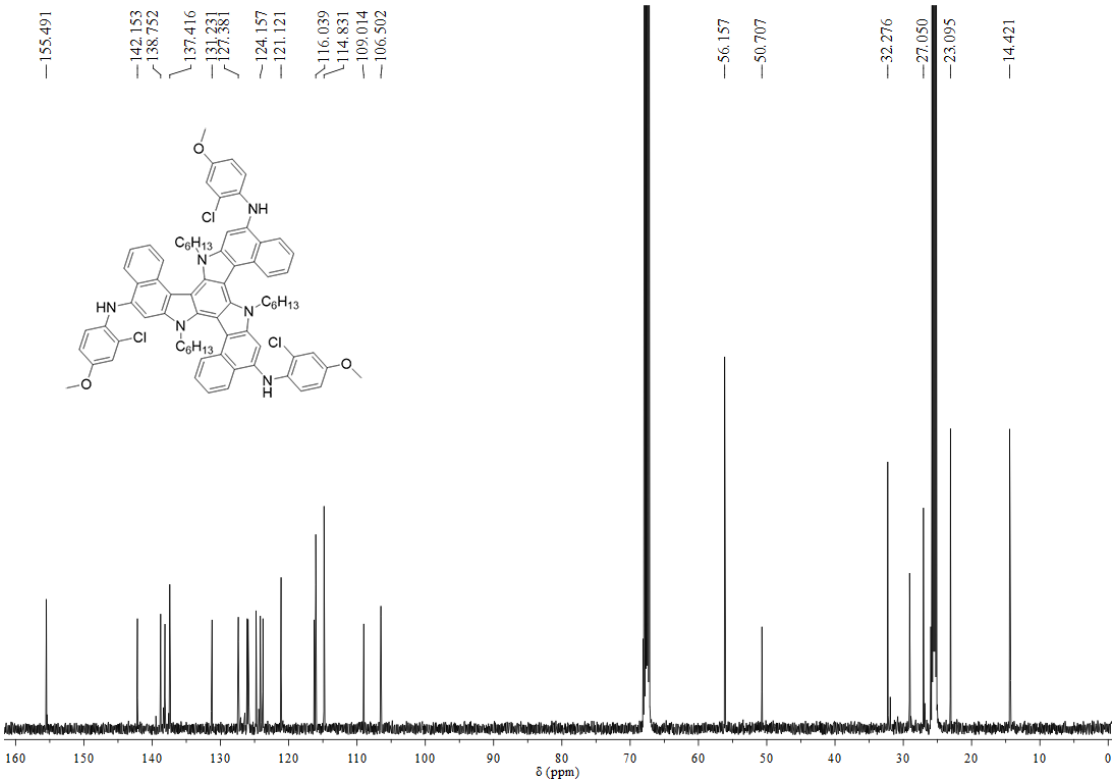

Fig. S44 The ^{13}C NMR (125 MHz) spectrum of 6 in THF-d_8.

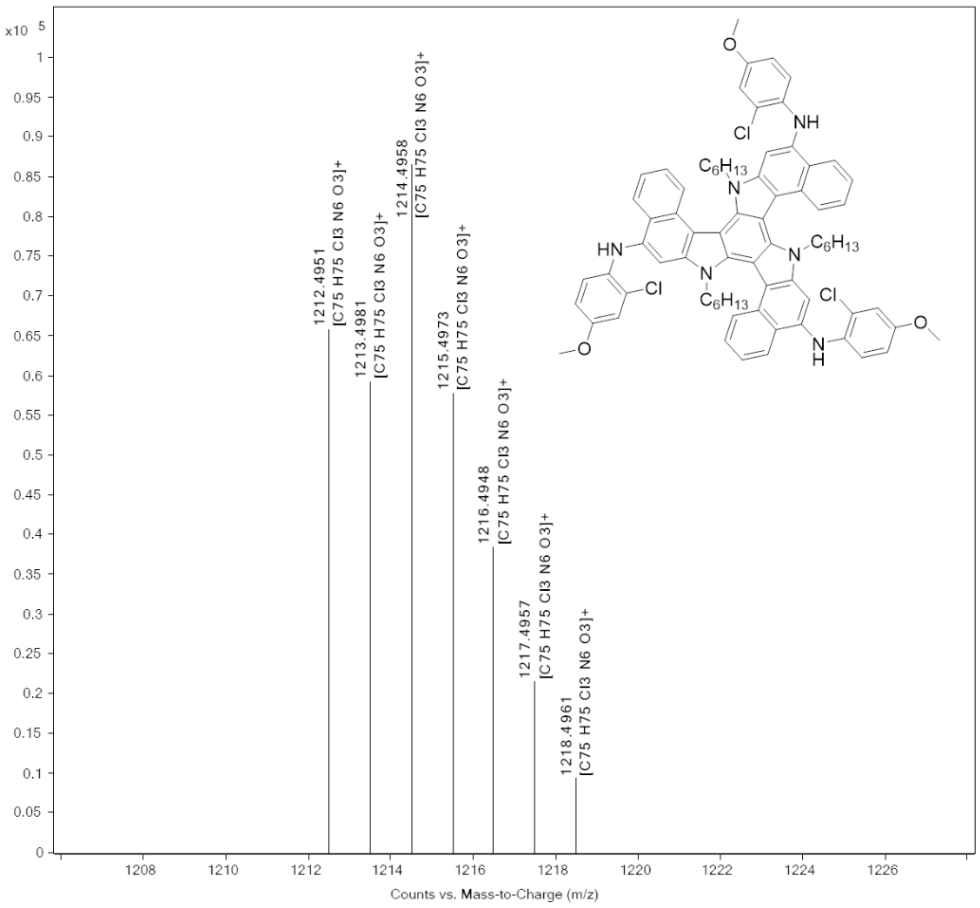

Fig. S45 The high-resolution mass spectrum (ESI) of 6.

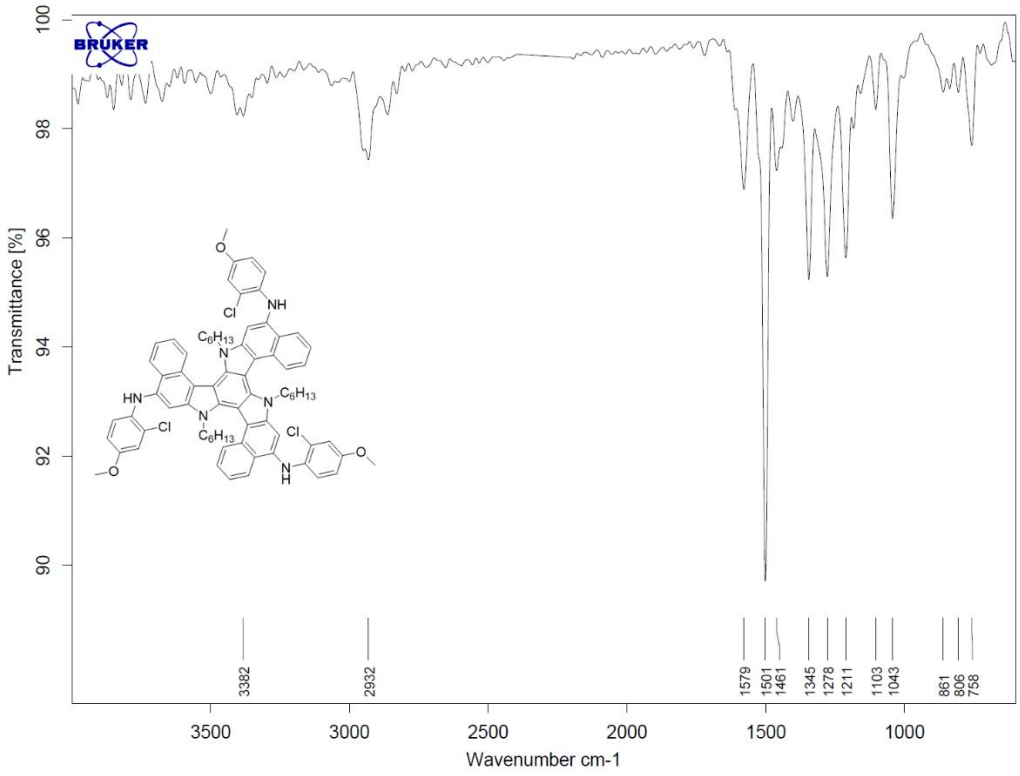

Fig. S46 The infrared spectrum of 6.

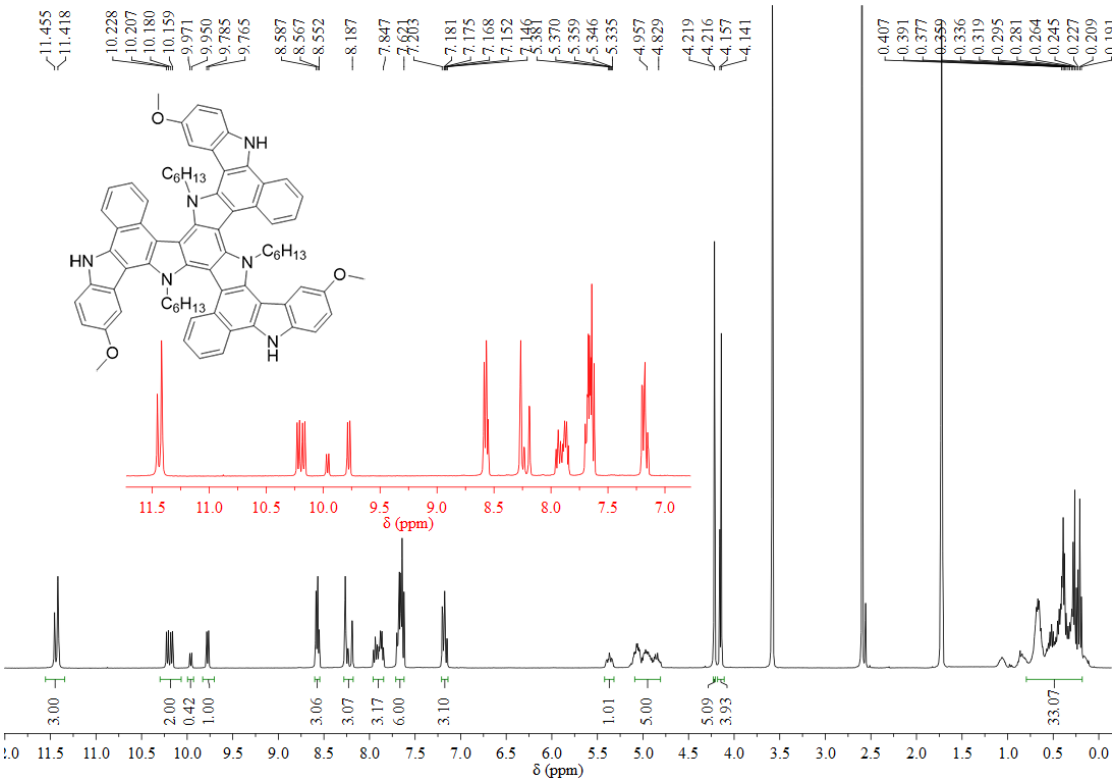

Fig. S47 The ^{1}H NMR (500 MHz) spectrum of 7 in THF-d_8.

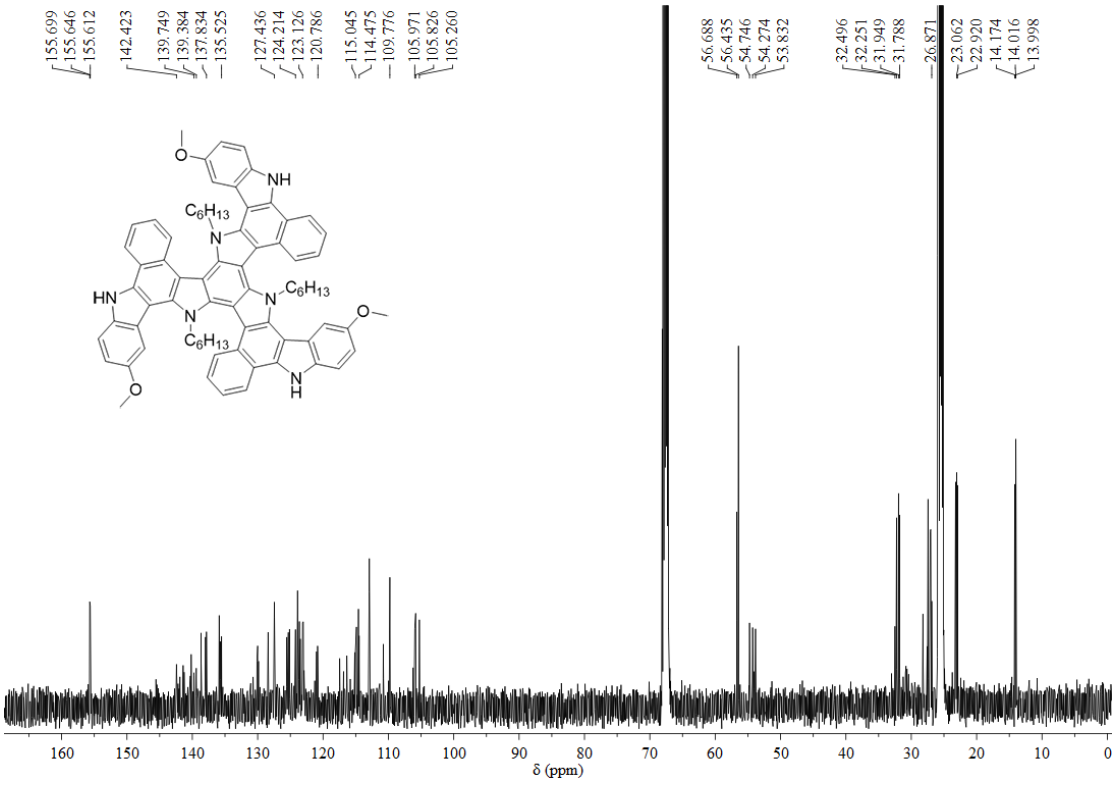

Fig. S48 The ^{13}C NMR (125 MHz) spectrum of 7 in THF-d_8.

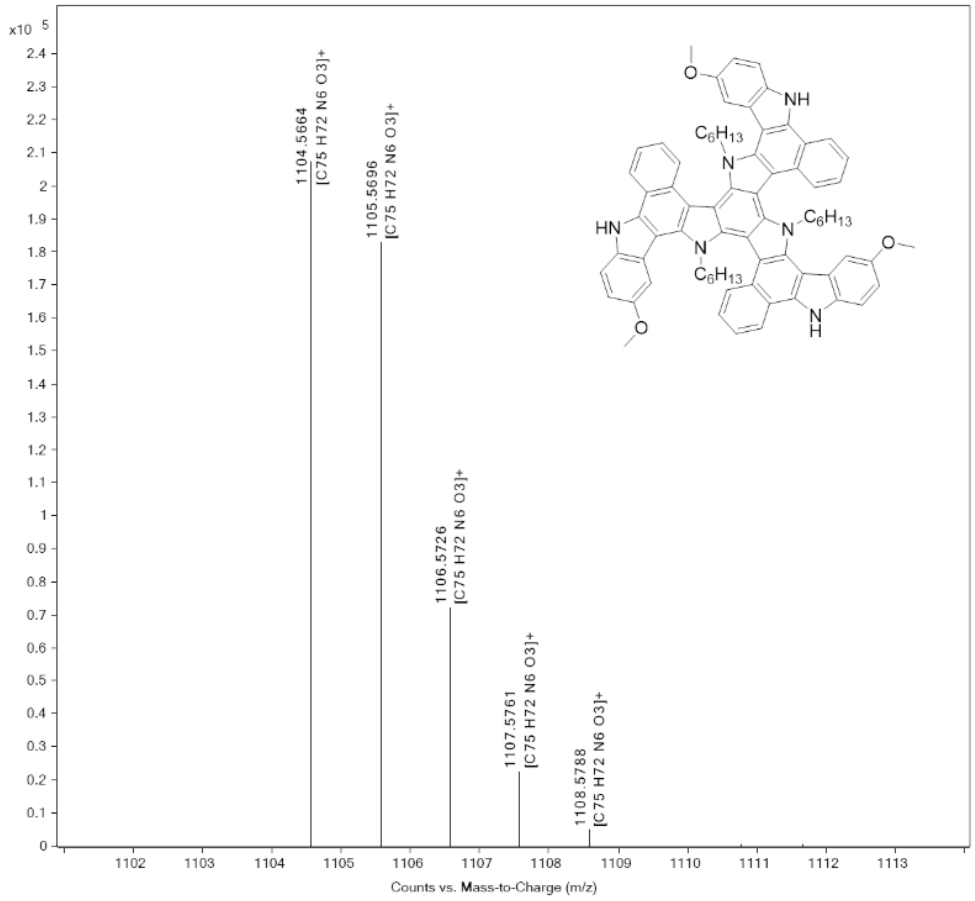

Fig. S49 The high-resolution mass spectrum (ESI) of 7.

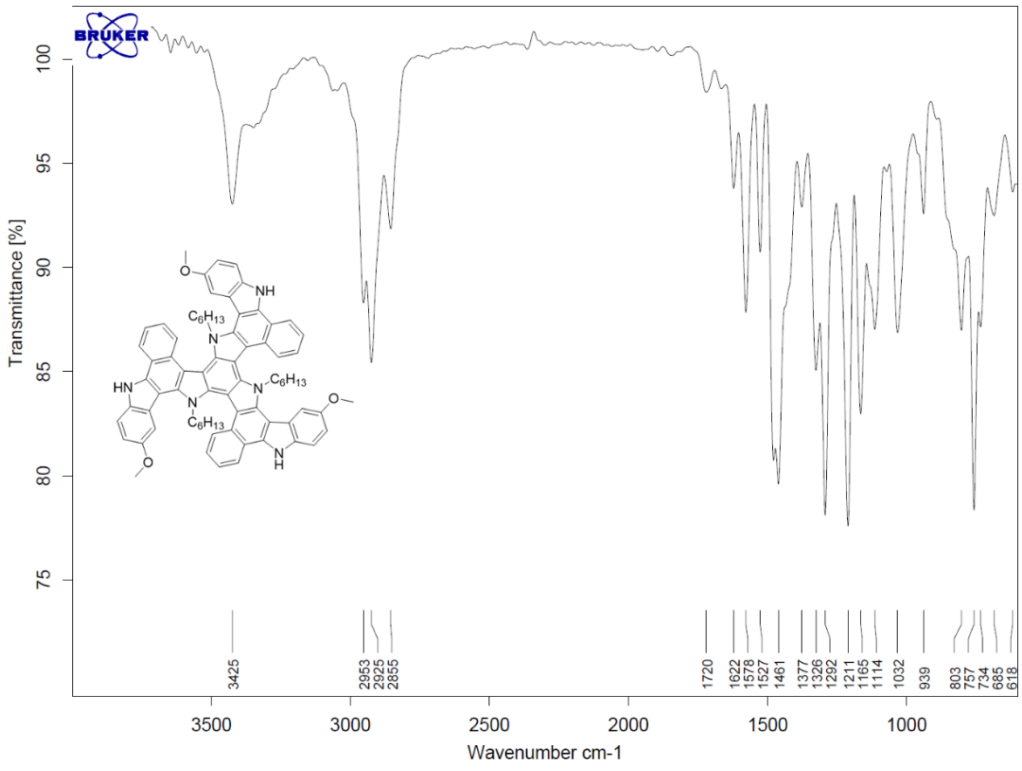

Fig. S50 The infrared spectrum of 7.

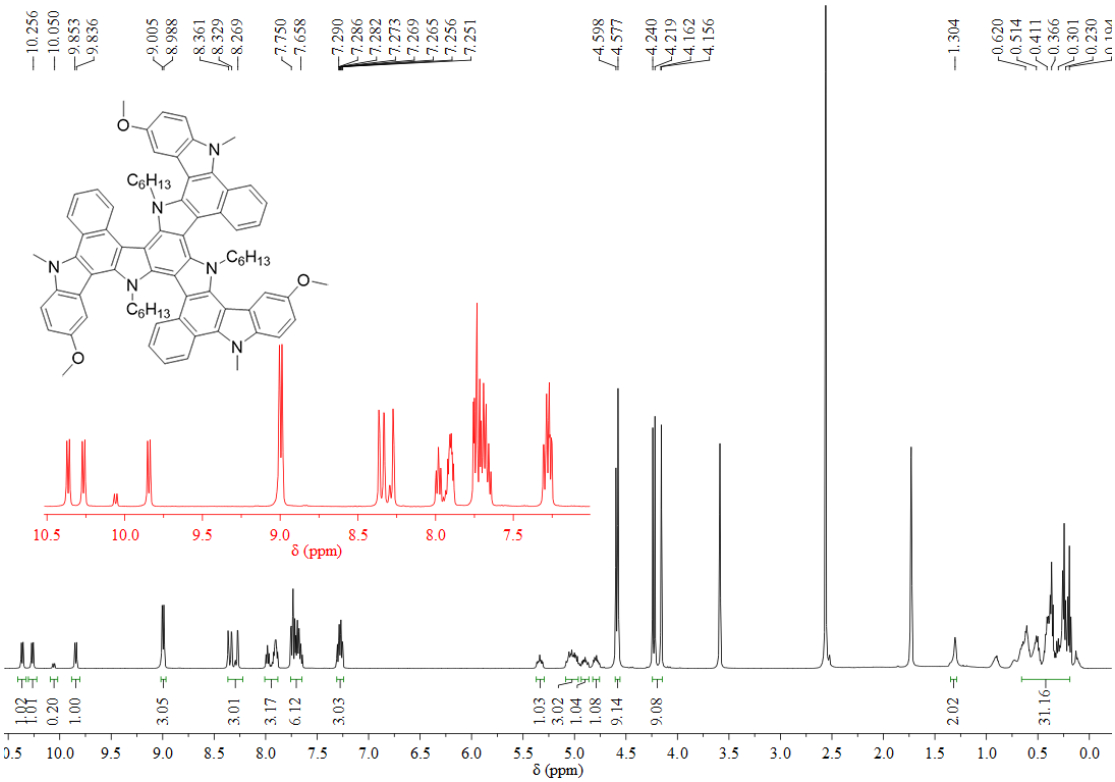

Fig. S51 The ^{1}H NMR (500 MHz) spectrum of TBPC-611 in THF-d_8.

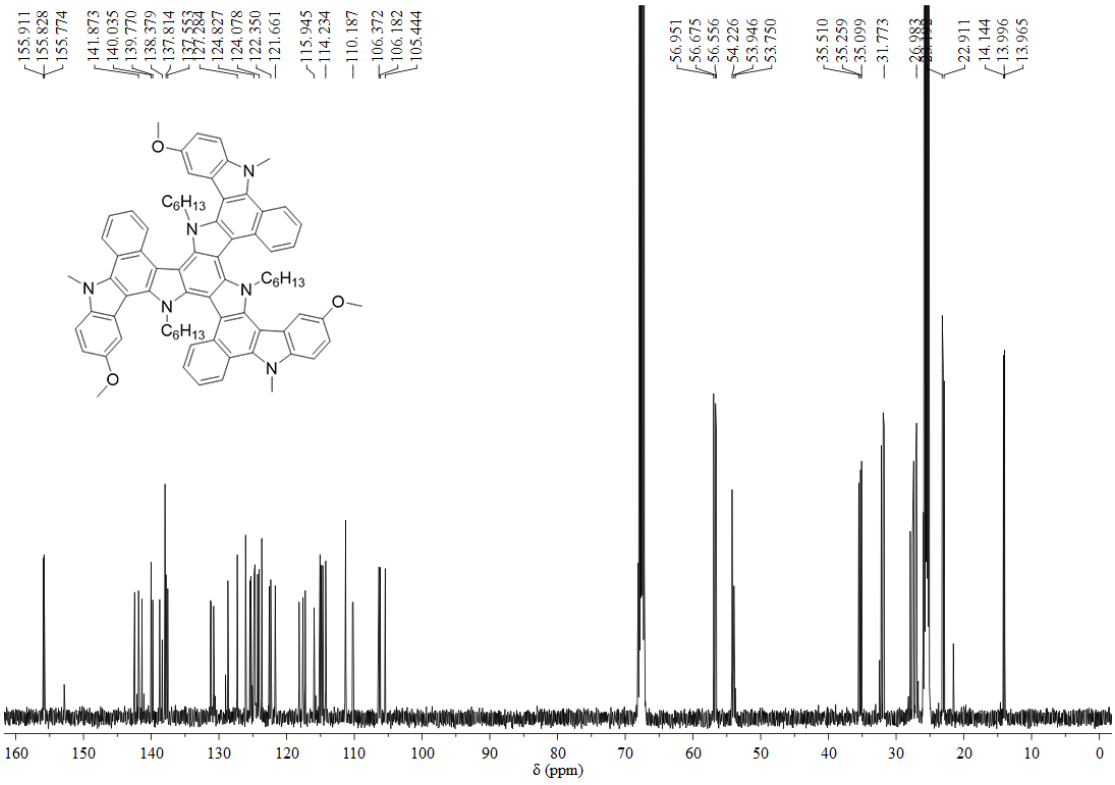

Fig. S52 The ^{13}C NMR (125 MHz) spectrum of TBPC-611 in THF-d_8.

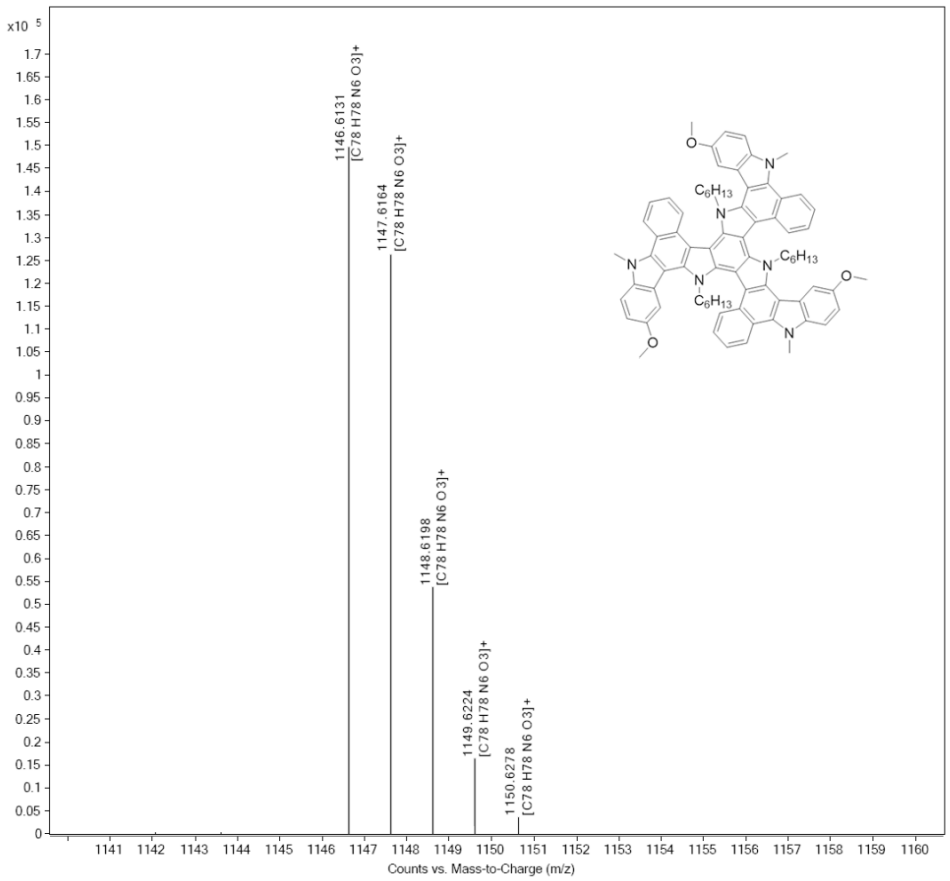

Fig. S53 The high-resolution mass spectrum (ESI) of TBPC-611.

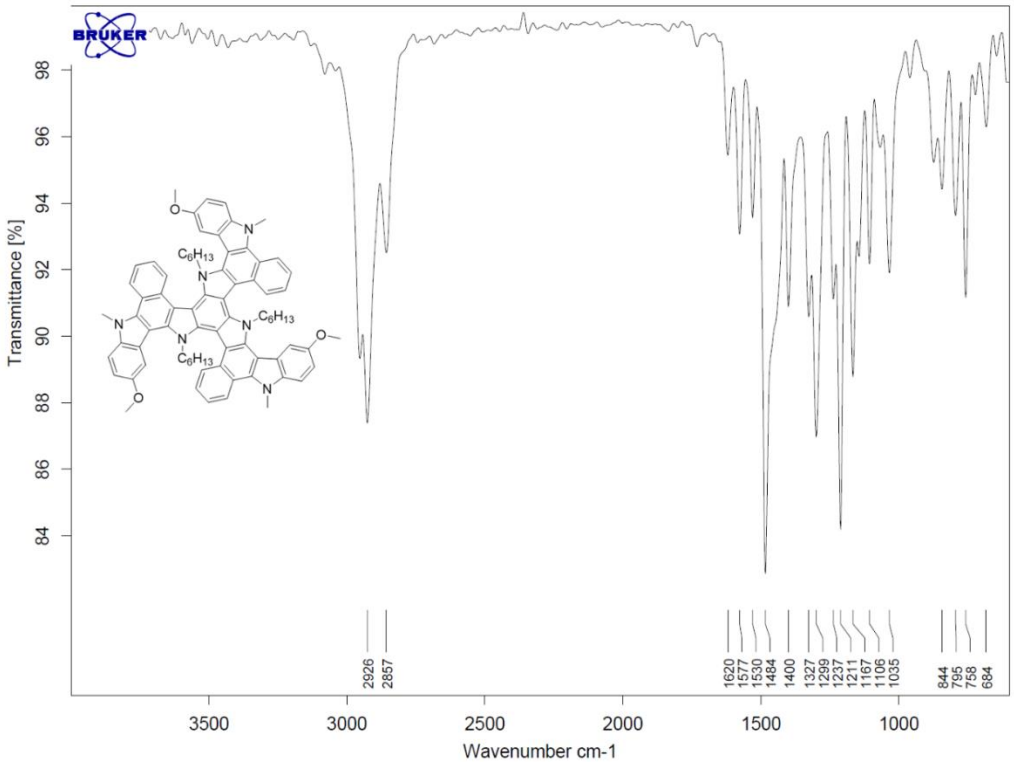

Fig. S54 The infrared spectrum of TBPC-611.